

Cite this: *J. Mater. Chem. A*, 2021, 9, 26628

Recent progress on post-synthetic treatments of photoelectrodes for photoelectrochemical water splitting

Yong Peng,^{ab} Chun Hong Mak,^{ab} Ji-Jung Kai,^c Minshu Du,^d Li Ji,^{*e} Mingjian Yuan,^f Xingli Zou,^{*g} Hsin-Hui Shen,^h Shella Permatasari Santoso,ⁱ Juan Carlos Colmenares^j and Hsien-Yi Hsu^{*ab}

For the global energy demand and climate change challenges, seeking renewable, sustainable energy sources is of great significance. Photoelectrochemical (PEC) water splitting is one of the promising technologies for converting intermittent solar energy into storable hydrogen energy, to tackle these issues. As the core component in a PEC system, photoelectrodes have been modified by various strategies including nanostructuring, facet-engineering, elemental doping, and heterostructured engineering. Apart from these techniques, numerous effective post-synthetic treatments have also been used to facilitate and powerfully boost the physicochemical properties of photoelectrodes, for the enhancement of their PEC performance. Among them, a number of post-treatments can selectively influence photoelectrode surface and subsurface areas, altering surface states that play crucial roles in the hydrogen/oxygen evolution reaction. In virtue of such post-treatments, we summarize recently reported post-synthetic treatments for enhanced PEC applications. Post-treatment methods are classified into three sections: chemical treatments, electrochemical and irradiation-based treatments, and post-annealing treatments. In the end, a summary and outlook section regarding the utilization of post-treatments for PEC applications have been provided. This review can provide inspiration for further studies about post-treatments, not only in the PEC water splitting field, but also in other aspects, such as electrolysis.

Received 14th July 2021
Accepted 8th November 2021

DOI: 10.1039/d1ta05935a

rsc.li/materials-a

1. Introduction

Hydrogen is envisioned as a clean, sustainable, and carbon-neutral energy source for the replacement of fossil fuels to meet the challenges of environmental concerns, the energy crisis, and global warming issues in the future. Converting intermittent solar energy to chemical energy stored in hydrogen is one of the promising technologies for large-scale hydrogen production by which to satisfy the ever-increasing energy demands of human society.^{25,26} It is estimated that capturing solar light at a solar-to-hydrogen (STH) efficiency of 10%, over an area of 250 000 km² which corresponds to only 1% of the earth's desert area, is required to fulfill one-third of the energy needs of the whole world in 2050.²⁷ In light of this, solar water splitting technologies—including but not limited to photovoltaic-based electrolysis (PV-E), photoelectrochemical (PEC) water splitting, and photocatalytic (PC) water splitting—have been developed.

The PV-E system primarily necessitates expensive photovoltaic devices, such as currently used silicon-based solar panels, for the conversion of solar energy to electricity. In comparison, PEC/PC water splitting, employing low-cost and effective photoresponsive materials, has drawn increased attention since the

^aSchool of Energy and Environment, Department of Materials Science and Engineering, City University of Hong Kong, Kowloon Tong, Hong Kong, China. E-mail: sam.hyhsu@cityu.edu.hk

^bShenzhen Research Institute of City University of Hong Kong, Shenzhen, 518057, China

^cDepartment of Mechanical Engineering, City University of Hong Kong, Kowloon Tong, Hong Kong, China

^dSchool of Materials Science and Engineering, Northwestern Polytechnical University, Xi'an, Shaanxi 710072, China

^eState Key Laboratory of ASIC and System, School of Microelectronics, Fudan University, Shanghai 200433, China. E-mail: lji@fudan.edu.cn

^fKey Laboratory of Advanced Energy Materials Chemistry (Ministry of Education), Renewable Energy Conversion and Storage Center (RECAST), College of Chemistry, Nankai University, Tianjin, 300071, P. R. China

^gState Key Laboratory of Advanced Special Steel, Shanghai Key Laboratory of Advanced Ferrometallurgy, School of Materials Science and Engineering, Shanghai University, Shanghai 200444, China. E-mail: xlzou@shu.edu.cn

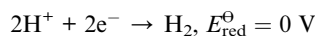
^hDepartment of Materials Science and Engineering, Faculty of Engineering, Monash University, Clayton, Victoria 3800, Australia

ⁱChemical Engineering Department, Widya Mandala Surabaya Catholic University, East Java, Indonesia

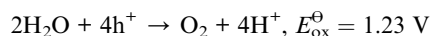
^jInstitute of Physical Chemistry, Polish Academy of Sciences, Kasprzaka 44/52, Warsaw 01-224, Poland. E-mail: jcarloscolmenares@ichf.edu.pl

seminal demonstration by Honda and Fujishima in 1972.²⁸ During PEC/PC water splitting, electrons in the valence band (VB) of a photocatalyst can be excited to the conduction band (CB) in response to light absorption.^{29–31} The photogenerated electrons and holes are then transported from the material bulk to its surface. Finally, the hydrogen evolution reaction (HER) and the oxygen evolution reaction (OER) can be realized at the surface of photoelectrodes and/or counter electrodes, respectively, as shown below.

HER:



OER:



Compared to PC water splitting, an extra small bias potential is generally required to be imposed on a single light-absorber photoelectrode, in order to overcome thermodynamic and kinetic barriers for PEC water splitting (compared to this, find ref. 32 for self-biased tandem cells for PEC water splitting). In spite of this, the PEC system has the advantage of separated hydrogen and oxygen gases, which avoids dangerous mixing and makes the system facile for studying various photoelectrodes.³³

In order to achieve practical PEC water splitting, the most important task is to develop efficient, robust, and cost-effective photoelectrodes. However, none of the present photocatalysts has satisfied all these requirements. There is no doubt about the importance of developing new cutting-edge photo-responsive materials for PEC applications, yet this process is certainly hard and rather time-consuming. On the other hand, engineering/modification of the existing materials to advance their bulk and surface/interface characteristics is feasible and useful. The bulk structure of photoelectrodes can be modulated by diverse strategies such as elemental doping, morphological engineering, facet regulating, heterojunction formation, and compositing engineering. Readers are directed to recently published excellent reviews, *e.g.*, ref. 32, 34 and 35.

Owing to the termination of lattice periodicity at the surface/interface, it is impossible to avoid a surface state that determines surface/interface properties in photoelectrodes.³⁶ Thus, an understanding of the surface state is of great significance to the development of practical PEC applications. In detail, overall PEC performance, *e.g.*, photocurrent density and solar-to-hydrogen efficiency, depends on the efficiencies of charge carrier formation, separation, and injection. The charge formation and separation characteristics are highly subjected to the intrinsic structural and electronic characteristics of the photoelectrodes. In comparison, surface states such as chemical surroundings, chemical bondings, or atomic arrangements, could be relatively easily altered with powerful post-synthetic treatments.

During PEC water splitting, HER and/or OER occur at the surface of photo-responsive materials. The interfacial properties

of semiconductor||semiconductor, semiconductor||overlayer, or photoelectrode||electrolyte can substantially affect the PEC response. Therefore, it is desirable to utilize post-synthetic approaches to modify the interface/surface properties of photoelectrodes, in pursuit of boosted solar-to-hydrogen conversion performance in an inexpensive and robust manner. In consideration of the abovementioned, we analyze studies related to post-synthetic treatments and PEC water splitting in the recent five years. In the review, we start with the introduction of facile chemical reduction and chemical modification methods, followed by a discussion of unique electrochemical and interesting irradiation-based treatments, as well as versatile post-annealing treatments, for improving the performance of photoelectrodes. Finally, we end with an outlook for future work.

2. Chemical treatments

Facile and effective chemical post-treatments can be used to modify photoelectrodes, which employ solution-based methods to process materials in most cases. This section is divided into two categories, chemical reduction and chemical modification. The major differences between these two methods are that chemical reduction employs reducing agents, such as sodium borohydride (NaBH_4), to react with photoresponsive materials in a vigorous manner. By comparison, chemical modifications are inclined to alter the surface states of the photoelectrodes *via* the formation of surface chemical bonds, without changing subsurface properties. Two points of view are emphasized as follows. (1) It is necessary to clarify that the classification for certain cases is somewhat subjective, due to the lack of a clear boundary. (2) It is worth noting that we have arranged solid- and gas-based chemical reduction cases in the post-annealing part, because it is normally essential to activate the reaction between solid photoresponsive materials with solid/gas reducing agents at high temperature and/or high pressure.

2.1 Chemical reduction

Reducing agents undergo rapid reactions with the photoelectrode surfaces. Chemical reduction is low-cost, fast and reliable, and therefore it is a popular chemical method to create oxygen vacancies of the metal oxide photoelectrode families.

2.1.1 Sodium borohydride. As a strong reducing agent, sodium borohydride (NaBH_4) has been extensively used to improve the photoactivity of various photoelectrodes, including TiO_2 , Fe_2O_3 , BiVO_4 , SrTiO_3 , Bi_2WO_6 , and BaSnO_3 .

Firstly, NaBH_4 treatment could conveniently create oxygen vacancies (O_{vac}) in photoelectrodes.^{37,38} Zheng *et al.* reported that O_{vac} could be introduced in black phosphorus (BP)-modified TiO_2 photoanodes by soaking them in a NaBH_4 aqueous solution.³⁷ The synergistic effect of O_{vac} and BP quantum dot sensitization was verified by PEC measurements. Notably, the generated O_{vac} and BP sensitization could not only facilitate charge separation but also enhance the water oxidation reaction, by improving the activity and quantity of reactive sites. In another study, Shi *et al.* explored the synergistic interaction between plasmonic Au nanoparticles and O_{vac} .³⁸ The

NaBH_4 -treated amorphous black TiO_2 photoanode maintained the O_{vac} , which could build intermediate energy levels. Such interband levels could facilitate the trapping and transfer of hot electrons generated from Au nanoparticles and thus improve electron-hole separation. *In situ* formation of surface heterophase could be realized using NaBH_4 .³⁹ Metallic Bi-modified O_{vac} -defective BiVO_4 photoanodes could be obtained by one-step NaBH_4 immersion treatment. The surface B-O bonds of BiVO_4 photoanodes were destructed and Bi^{3+} atoms were reduced to Bi^0 nanocrystals. At the same time, the formed O_{vac} could significantly enhance charge carrier separation and benefit the adsorption of water molecules, while the metallic Bi nanocrystals facilitate charge separation and consumption, due to the surface plasmon resonance effect.

In situ formation of the FeB overlayer on Fe_2O_3 could be generated by dipping the photoanode in an aqueous NaBH_4 solution.⁴⁰ The FeB layer could suppress charge carrier recombination in Fe_2O_3 and reduce interfacial resistance of electrode|electrolyte. In view of this, a twofold increase in photocurrent density could be observed. In comparison to this study,⁴⁰ another report on the NaBH_4 treatment of Fe_2O_3 showed that modification of NaBH_4 only contributed to a slight enhancement of photocurrent density.¹² However, it is interesting to find that, with both NaBH_4 treatment and Co-Pi coating, the onset potential of the as-prepared Co-Pi/ Fe_2O_3 - NaBH_4 photoanode decreased by 210 mV, compared to 110 mV of Co-Pi/ Fe_2O_3 . NaBH_4 could induce surface states that serve as surface charge transfer and recombination sites. After Co-Pi coating, such surface states not only stored the accumulated holes but also served as a block layer to prevent the recombination of photogenerated electrons with the oxidation intermediates in the Co-Pi cocatalyst (Fig. 1).

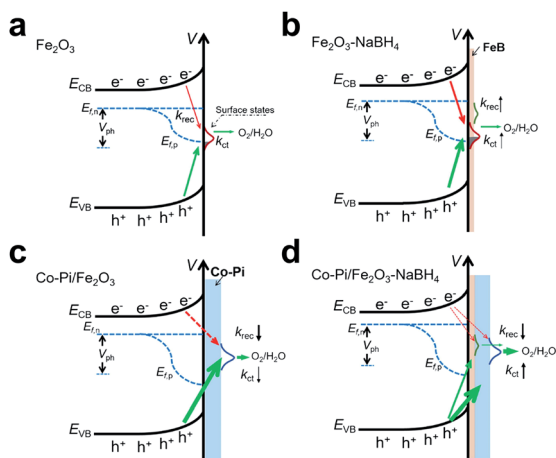


Fig. 1 (a) Charge transfer pathway in bare Fe_2O_3 , (b) NaBH_4 treatment could induce surface states that serve as surface charge transfer (k_{ct}) and recombination (k_{rec}) sites, (c) only Co-Pi coating decreased the recombination rate (k_{rec}) but unfavorably impaired charge transfer (k_{ct}), (d) after coating Co-Pi on NaBH_4 -treated Fe_2O_3 , surface states not only stored accumulated holes but also served as block layer to prevent recombinations.¹² Reprinted with permission from ref. 12, copyright 2019 Elsevier Inc.

NaBH_4 treatments are also beneficial to bimetallic oxide semiconductors, such as strontium titanate (SrTiO_3),^{2,17,41} bismuth tungstate (Bi_2WO_6),⁴² and barium stannate (BaSnO_3).⁴³ Shi *et al.* reported the formation of crystalline-core@amorphous-shell structured SrTiO_3 photoelectrodes by NaBH_4 treatment at 320 °C.² Owing to the localized surface plasmon resonance effect and the high carrier density induced by O_{vac} , the treated photoanode exhibited an enhanced photocurrent density of 170 $\mu\text{A cm}^{-2}$ under AM 1.5 G with an L-42 cutoff filter (Fig. 2a-c). Similarly, with NaBH_4 to process TiO_2 / SrTiO_3 heterostructure,¹⁷ surface amorphous structure and O_{vac} could be generated, which benefited the adsorption of hydroxide ions as well as the transfer of charge carriers (Fig. 2d). In addition to SrTiO_3 , O_{vac} of Bi_2WO_6 could be prepared by a simple NaBH_4 etching process.⁴² The presence of O_{vac} could decrease charge transfer resistance and thus increase photocurrent density. It is worth noting that an inappropriate amount of NaBH_4 could create excessive O_{vac} , which could serve as charge carrier recombination centers, undermining the photoactivity of the Bi_2WO_6 photoanode. Recently, Kim *et al.* reported that solution-based NaBH_4 treatment could induce O_{vac} in BaSnO_3 photoanodes, gradually narrowing the bandgap of BaSnO_3 from 3.11 eV to 1.81 eV.⁴³ The amount of O_{vac} could be

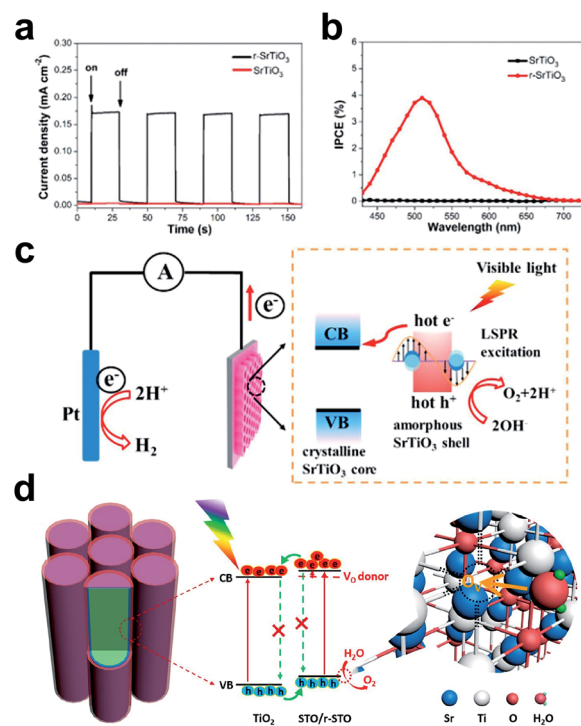


Fig. 2 (a) Transient photocurrent responses and (b) IPCE values of SrTiO_3 and $r\text{-SrTiO}_3$ photoelectrodes at 1.23 V vs. RHE with an L-42 cutoff filter, and (c) localized surface plasmon resonance effect enhanced PEC water splitting of SrTiO_3 under visible light.² Modified with permission from ref. 2, copyright 2018 American Chemical Society. (d) Schematic illustration of the synergistic effects between close contact TiO_2 / SrTiO_3 heterojunction and NaBH_4 -induced surface O_{vac} .¹⁷ Reprinted with permission from ref. 17, copyright 2019 American Chemical Society.

precisely controlled, and the BaSnO_3 photoanode with 8.7% of O_{vac} exhibited the highest light absorption and best charge separation performance. After further coating $\text{FeOOH}/\text{NiOOH}$ layered double oxide, this photoanode exhibited a remarkable photocurrent of 7.32 mA cm^{-2} at 1.23 V vs. RHE .

2.1.2 Other reducing agents. In addition to sodium borohydride, a number of reducing agents such as lithium metal dissolved in ethylenediamine (Li-EDA), titanium(III) chloride (TiCl_3), sodium hypophosphite (NaH_2PO_2), and sodium sulfite (Na_2SO_3) have been used to modify the surface atomic arrangements and/or surface states of photoelectrodes.

Li-EDA, as a strong reducing agent, has been employed to process TiO_2 ³ and BiVO_4 .¹⁴ Zhang *et al.* reported the formation of a controllable crystal-deficient overlayer in rutile TiO_2 arrays by facile immersion in liquid Li-EDA for 5–120 s (Fig. 3a–e).³ The created overlayer not only resulted in enhanced light absorption but also improved the conductivity of TiO_2 by 50 times, benefiting electron collection in the photoanode. As a result, the as-obtained TiO_2 photoanode exhibited a photocurrent density of 2.0 mA cm^{-2} at 1.23 V vs. RHE , four times higher than that of bare TiO_2 . Likewise, another study indicated that Li-EDA could induce the subsurface alteration of atomic arrangement in BiVO_4 (Fig. 3f and g).¹⁴ The disordered surface layer, generated

by a 5 s Li-EDA treatment, could alleviate charge carrier recombination at the $\text{BiVO}_4/\text{electrolyte}$ interface, leading to the increase of photocurrent density by 2.1 times. The enhanced charge separation and charge transfer properties were responsible for the improved photoactivity of the Li-EDA-treated BiVO_4 photoanode. Kim *et al.* demonstrated the effectiveness of a TiCl_3 -mediated treatment for TiO_2 nanotubes.⁴⁴ Both surface O_{vac} and the TiO_2 nano-branch layer could be generated with the post-treatment, which resulted in an improved charge carrier density and strengthened surface roughness, respectively. As a result, the photocurrent density increased from 0.83 mA cm^{-2} to 2.25 mA cm^{-2} at 1.23 V vs. RHE . Another report by Liu *et al.* revealed that the concentration of O_{vac} in WO_3 photoanodes could be controlled and was proportional to the amount of TiCl_3 .⁴⁵ Enhanced PEC activity could be observed after treatments with certain concentrations of TiCl_3 , otherwise excessive O_{vac} might be generated to serve as surface defects for charge carrier recombination, resulting in unsatisfactory separation and transfer of charge carriers.

Yang *et al.* investigated the thermodynamic and kinetic influence of O_{vac} on Fe_2O_3 photoanodes.⁴⁶ Sodium hypophosphite (NaH_2PO_2) was used as a reductant to induce various amounts of O_{vac} in the photoanodes by adjusting the time of

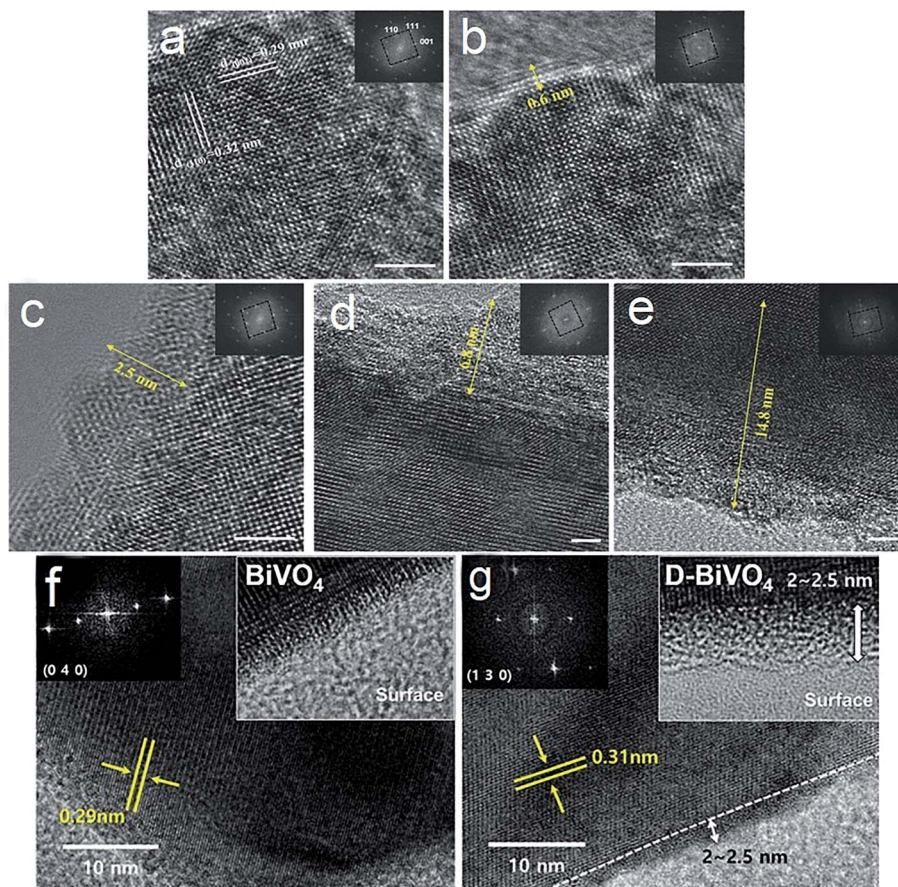


Fig. 3 (a–e) TEM images of Li-EDA-treated TiO_2 nanowires for 5, 10, 20, 60, and 120 s, respectively. Scale bars 2 nm. Insets are the FFT converted from the corresponding TEM images.³ (f and g) TEM images of (f) bare BiVO_4 and (g) Li-EDA treated BiVO_4 .¹⁴ Modified with permission from ref. 3 and 14, copyright 2016 and 2018, respectively, WILEY-VCH Verlag GmbH & Co. KGaA, Weinheim.

hydrothermal reactions. Notably, a prolonged time of 180 min could induce unfavorable bulk O_{vac} which had a negative effect on the photoactivity of Fe_2O_3 . In comparison, the presence of surface O_{vac} decreased space charge region width, resulting in boosted charge separation and transfer. Additionally, from the perspective of kinetics, the surface O_{vac} could also improve the surface properties and hydrophilicity of the Fe_2O_3 photoanodes. In a similar manner, our group employed a mild reducing agent, sodium sulfite (Na_2SO_3), to modify the surface properties of the $BiVO_4$ photoanodes.⁴⁷ The facile immersion of $BiVO_4$ films in the Na_2SO_3 aqueous solution could create surface O_{vac} and disordered surface structure. Owing to the decreased charge carrier recombination, the as-prepared sulfite-treated $BiVO_4$ exhibited a photocurrent density of 2.2 mA cm^{-2} at 1.23 V vs. RHE, 1.7 times higher than that of bare $BiVO_4$. In addition to inorganic compounds, organic compounds could also be useful for chemical reduction treatments. For example, Long *et al.* reported the use of ethylene glycol for the reduction of CoO_x -coated ZnO nanorods.⁴⁸ After solvothermal reaction at 140 °C for 8 h, the amount of O_{vac} in the photoelectrode was substantially increased, which acted as favorable trapping

centers for the migration of photogenerated holes at the electrode|electrolyte interface. Consequently, the reduced CoO_x -coated ZnO photoanode exhibited a photocurrent density of 2.1 mA cm^{-2} , 2.1 times higher than that of bare ZnO nanorods and 1.6 times higher than that of the CoO_x -coated ZnO ones.

Studies of the above chemical reduction treatments have been summarized in Table 1. It is facile and effective to employ chemical reduction methods for the post-treatments of various photoelectrodes. The physicochemical properties of the material, especially of the subsurface, can be selectively altered, depending on specific treating parameters. In most cases, an undesired structure (*e.g.*, excessive O_{vac}) could be created with an excessive amount of reducing agents or reaction time. Therefore, adjusting reaction parameters (*e.g.*, concentration of reducing agents, reaction time, and temperature) or employing other practical methods to precisely control the reaction process are expected. In addition, since the reducing agents used in the reported studies are primarily inorganic compounds, it might be suggested to screen suitable organic compounds as reducing agents to modify photoelectrodes for the pursuit of stable and effective photoactivity.

Table 1 Chemical reduction of photoelectrodes for enhanced PEC performance

Materials	Post-treatments	Photocurrent density ($\alpha \text{ mA cm}^{-2}$ at $\beta \text{ V vs. } \gamma; \delta \text{ times}$) ^c	Ref.
NaBH₄			
BP ^a /TiO ₂	Soaked in 0.1 M NaBH ₄ for 10–70 min	1.12; 1.23; RHE; 3.0	37
TiO ₂	Mixed with NaBH ₄ and heated at 360 °C for 2 h	1.33; 1.23; RHE; 3.1	38
BiVO ₄	0.5 g of BiVO ₄ powders dispersed into 50 mL of 20 mg mL ⁻¹ NaBH ₄ and stirred for 30–60 min	1.00; 1.23; RHE; 8.3	39
Fe ₂ O ₃	Dipped in 0.1 M NaBH ₄ for 40 min	1.65; 1.23; RHE; 2.2	40
Fe ₂ O ₃	Immersed in 0.2 M NaBH ₄ for 10–30 min, followed by loading Co-Pi cocatalysts	1.29; 1.23; RHE; 1.5	12
SrTiO ₃	Mixed with 0.5 g of NaBH ₄ and heated at 320 °C for 2 h in N ₂	1.71; 1.23; RHE; 3.1	2
TiO ₂ /SrTiO ₃	Covered by 0.22 g of NaBH ₄ and heated at 320 °C for 2 h in Ar	0.32; 1.23; RHE; 1.5	17
Bi ₂ WO ₆	0.4 g of Bi ₂ WO ₆ in 50 mL H ₂ O mixed with 2.5–10 mL of 0.8 g L ⁻¹ NaBH ₄ under N ₂ for 3 h	1.90; 1.23; RHE; 2.7	42
BaSnO ₃	0.5 g of BaSnO ₃ immersed in 130 mL of 1–7 M NaBH ₄ for 3 h followed by coating FeOOH/NiOOH cocatalysts	7.32; 1.23; RHE; 7.3	43
Li-EDA^b			
TiO ₂	Immersed in 0.69 mg mL ⁻¹ of Li-EDA ^b for 5–120 s	1.70; 1.23; RHE; 3.4	3
BiVO ₄	Immersed in 0.05 M of Li-EDA ^b for less than 5 s	2.30; 1.23; RHE; 2.1	14
TiCl₃			
TiO ₂	Immersed in 10 mL of 17–68 mM of TiCl ₃ at 60–100 °C for 5–40 min	2.25; 1.23; RHE; 2.7	44
WO ₃	Dipped in 50–200 mg L ⁻¹ of TiCl ₃ for 25 s	0.82; 1.2; Ag/AgCl; 1.27	45
NaH₂PO₂			
Fe ₂ O ₃	Hydrothermally heated in 1 M NaH ₂ PO ₂ at 100 °C for 60–180 min	2.40; 1.6; RHE; 1.8	46
Na₂SO₃			
BiVO ₄	Immersed in 0.2 M Na ₂ SO ₃ at 60 °C for 24 h	2.20; 1.23; RHE; 1.7	47
Ethylene glycol			
CoO _x /ZnO	Hydrothermally heated in 5 mmol NaOH dissolved in 10 mL ethylene glycol at 140 °C for 8 h	2.10; 1.23; RHE; 1.3	48

^a BP: black phosphorus. ^b Li-EDA: lithium metal dissolved in ethylenediamine. ^c Photocurrent density ($\alpha \text{ mA cm}^{-2}$ at $\beta \text{ V vs. } \gamma; \delta \text{ times}$) = 1.12; 1.23; RHE; 3.0, for example, means 1.12 mA cm^{-2} at 1.23 V vs. RHE, 3.0 times higher than the photocurrent density of relevant untreated sample, similarly hereafter.

2.2 Chemical modification

In comparison to the occurrence of strong reactions between reducing agents and photoelectrodes, the surface alteration induced by chemical modification can usually be rather slow and gentle. Chemical modification methods, including acid and alkaline treatments, contact-induced surface alternations, and *in situ* ion exchange are summarized as follows.

2.2.1 Acid and alkaline treatments. Facile acid or alkaline treatments have been used for effectively improving the PEC performance of hematite. Yang *et al.* immersed Fe_2O_3 photoanodes in pure acetic acid (CH_3COOH) for 5 min, followed by calcination treatment.⁴⁹ The acid-treated Fe_2O_3 exhibited a considerably increased photocurrent density, from 0.3 mA cm^{-2} of bare Fe_2O_3 to 1.2 mA cm^{-2} at $0.2 \text{ V vs. Ag/AgCl}$, which was ascribed to the decreased charge recombination loss arising from an improved detrapping rate. The reduced charge recombination rate was also consistent with the observation of improved conductivity and enhanced charge separation efficiency. In addition to acetic acid, employing other acids, including HCl , HNO_3 , and H_3PO_4 for the post-treatment, could also improve the photoactivity of Fe_2O_3 photoanodes. As a comparison, other studies have indicated that the primary reason for the effectiveness of acid treatment should be the passivation of surface states⁵⁰ or the suppression of back reactions.⁵¹ Apart from acid treatments, Zhang *et al.* reported the use of the alkaline solution for the modification of Fe_2O_3 .⁵² Spin-coating KOH solution on Fe_2O_3 followed by annealing could effectively modify the surface of Fe_2O_3 with numerous hydroxyl groups. The hydroxyl overlayer exhibited electrocatalyst-like properties, which accelerated water oxidation kinetics. Moreover, the valence band of the alkaline-treated Ti-doped Fe_2O_3 increased by 0.15 eV , indicating *in situ* formation of a type II heterojunction along with the introduction of the hydroxyl-rich overlayer. In contrast to this method, the direct immersion of Fe_2O_3 in 1 M KOH was reported for self-passivation.⁵³ In view of the passivating effect, improved donor density and increased surface charge transfer properties could be observed, which contributed to enhanced photoactivity.

In addition to Fe_2O_3 , photoelectrodes such as TiO_2 , CaTaO_2N , and ZrO_2 have also been treated with acid for PEC applications. Mao *et al.* reported the use of nitric acid for the treatment of TiO_2 to introduce oxygen defects in the photoanode.⁵⁴ The induced oxygen defects could improve the intrinsic conductivity of the TiO_2 photoanode, resulting in an enhancement in donor density. As a result, the acid-treated TiO_2 exhibited a photocurrent density of 2.8 mA cm^{-2} at $0.23 \text{ V vs. Ag/AgCl}$, 2.5 times higher than that of pristine TiO_2 . In comparison, the surface properties of CaTaO_2N powders could be considerably altered with the treatment of aqua regia for only 20 s.⁵⁵ As characterized by ^1H and ^{14}N solid-state nuclear magnetic resonance (NMR), the generation of abundant OH groups at the restructured surface of CaTaO_2N could be detected. The acid modification strategy resulted in an enhanced surface charge transfer efficiency in the CaTaO_2N photoanode and yielded an increased photocurrent density by approximately four times. Another study by Rahman *et al.* demonstrated the effectiveness

of using hydrofluoric (HF) acid for the treatment of ZrO_2 hierarchical nanowires.⁵⁶ The HF acid treatment enabled the generation of thin amorphous ZrO_2 shells on crystalline ZrO_2 . As a result, an enhanced charge transport property and increased electrochemically active sites were obtained, along with the formation of O_{vac} . Consequently, the treated ZrO_2 nanowires exhibited a significantly improved photocurrent density of -42.5 mA cm^{-2} at 0 V vs. RHE , in comparison to -12.9 mA cm^{-2} of pristine ZrO_2 nanowires. Additionally, this simple post-treatment method could also be utilized to treat other photoelectrodes such as TiO_2 and Ta_2O_5 for efficient PEC performance.

2.2.2 Contact-induced surface alternations. Contact-induced surface alternation using both inorganic and organic compounds has been widely reported. Wang *et al.* investigated the influence of surface fluorine-modification on Fe_2TiO_5 photoanodes.¹⁰ After immersing Fe_2TiO_5 films in a $\text{NH}_4\text{F}/\text{H}_2\text{O}_2$ solution followed by an annealing process, Ti-F bonds on the surface could be created, as demonstrated by XPS analysis (Fig. 4a–d). The generated Ti-F bonds could facilitate the hole transfer process and approximately doubled the photocurrent density, at 1.23 V vs. RHE . Another report explored the synergistic effects of F- and Rh-based treatments on heterostructured $\text{Fe}_2\text{TiO}_5/\text{Fe}_2\text{O}_3$ photoanodes.⁵⁷ Similar to the above, F-treatment also employed the $\text{NH}_4\text{F}/\text{H}_2\text{O}_2$ immersion method followed by calcination, while Rh,F-treated samples were prepared by Rh-treatment—a photoassisted electrodeposition method. The F-treatment could modify the interface structure with the hydrogen-bond network for fast hole transfer, while the Rh-

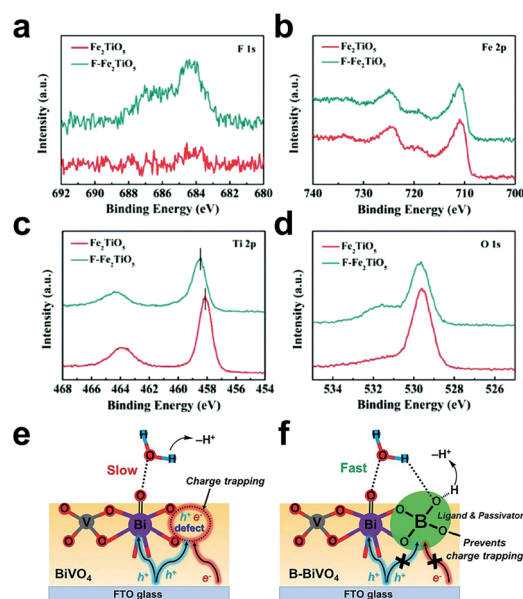


Fig. 4 (a) F 1s, (b) Fe 2p, (c) Ti 2p and (d) O 1s XPS spectra of pristine Fe_2TiO_5 (red line) and surface F-modified Fe_2TiO_5 (green line).¹⁰ Reprinted with permission from ref. 10, copyright 2018 The Royal Society of Chemistry. (e and f) Tetrahedral $[\text{B}(\text{OH})_4]^-$ species as regulating ligand and passivator to accelerate hole transfer and reduce charge trapping: (e) without and (f) with borate modification.¹⁹ Modified with permission from ref. 19, copyright 2019 The Authors.

treatment enhanced catalytic performance. In addition to fluorine ions, other common ions, such as phosphate (PO_4^{4-}) and borate (BO_3^{3-}) ions, can also be effective for surface modification. Meng *et al.* reported the immersion of BiVO_4 photoanodes in a borate buffer solution at room temperature.¹⁹ Remarkably, the borate-treated BiVO_4 photoanode exhibited an onset potential shift of 320 mV and a substantially enhanced photocurrent density of 3.5 mA cm^{-2} at 1.23 V vs. RHE, compared to 1.6 mA cm^{-2} of the pristine BiVO_4 .

Their characterizations indicated that the bulk nature of the BiVO_4 photoanode remained unchanged after the post-treatment, while the reason for enhanced PEC performance was ascribed to the absorption of tetrahedral $[\text{B}(\text{OH})_4]^-$ species near the active sites, which served as a regulating ligand and passivator to accelerate hole transfer and reduce charge trapping during water oxidation reaction (Fig. 4e and f). It is worth noting that the surface structure may not be so stable, as overnight immersion in pure water could undermine the PEC performance of the treated BiVO_4 . In another report, phosphate ions were exploited to functionalize Ti-doped Fe_2O_3 photoanodes by a cost-effective dip-annealing method.⁵⁸ The photoanodes were post-treated with immersion into a Na_3PO_4 solution followed by calcination in N_2 . This phosphate functionalization not only lowered the onset potential by suppressing electron-hole recombination, but also improved surface water oxidation kinetics, resulting in an enhancement in photocurrent density. Likewise, Sahu *et al.* reported the co-modification of Fe_2O_3 photoanodes by titanium doping and phosphate treatment.⁵⁹ The co-modification significantly improved the photocurrent density from 0.45 mA cm^{-2} of untreated Fe_2O_3 to 2.56 mA cm^{-2} of co-modified Fe_2O_3 , arising from the increased charge carrier density (10 fold) and improved charge transfer characteristic. With the introduction of light treatment, the interaction between phosphate ions and BiVO_4 photoanodes was studied.⁶⁰ A 25–30 nm thick layer was generated with a dip-and-pull method under illumination, which led to the formation of bismuth phosphate endowed with a negative charge. Interestingly, such a negatively charged structure may function as a passivation layer for the deactivation of surface states of BiVO_4 , revealing the importance of selecting a suitable electrolyte for practical PEC water splitting.

In addition to inorganic compounds, employing organic matter such as methanol, 1,2-ethanedithiol, and thioacetamide for chemical modification is also efficacious. For example, Xiao *et al.* explored the roles of distinct surface defects generated by methanol or HCl treatments in Fe_2O_3 photoanodes.¹ Interestingly, methanol treatment at 180 °C for 10 h induced a hydroxylated surface on Fe_2O_3 , while HCl treatment at 95 °C for 1 h created abundant chemisorbed oxygen on the photoanode. Methanol treatment improved the charge carrier density and surface hydrophilicity of Fe_2O_3 , resulting in enhanced photoactivity. In contrast, HCl treatment barely affected carrier density and hydrophobicity. Instead, surface states were altered with the treatment of HCl, which promoted surface charge transfer and suppressed bulk recombination of charge carriers, thereby lowering the onset potential (Fig. 5a). The photocurrent density of the photoanode was optimized to 3.0 mA cm^{-2} at

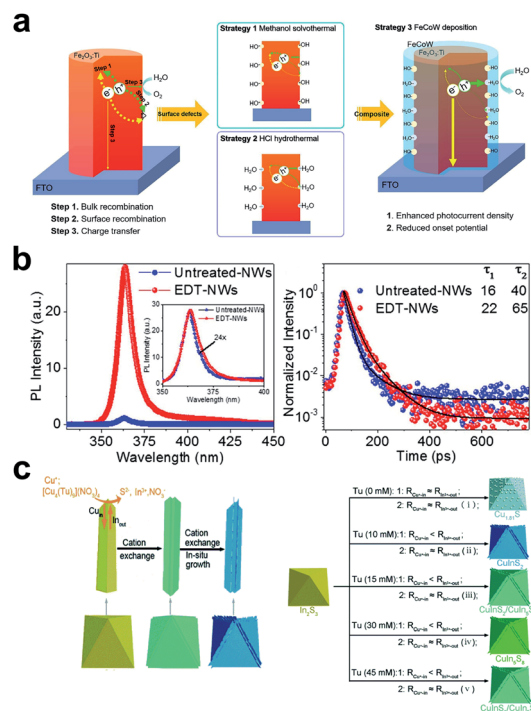


Fig. 5 (a) Schematic illustration of surface states induced by methanol and HCl treatments as well as the combination with the cocatalyst FeCoW to enhance PEC performance.¹ Reprinted with permission from ref. 1, copyright 2020 Elsevier B.V. (b) Room-temperature photoluminescence and time-resolved photoluminescence spectra of untreated and EDT-treated GaN nanowires.¹³ Reprinted with permission from ref. 13, 2017 American Chemical Society. (c) Schematic illustration of the formation mechanism for grooved pyramid-like morphology (left), and the generation of various structures by maneuvering the rate of cation exchange with an increased amount of thiourea (right).²³ Modified with permission from ref. 23, copyright 2018 The Royal Society of Chemistry.

1.23 V vs. RHE with the addition of cocatalysts. Varadhan *et al.* employed 1,2-ethanedithiol (EDT) for the surface passivation of GaN nanowires.¹³ A 5 min EDT treatment followed by loading Pt cocatalyst could improve the charge carrier separation efficiency of the photocathode by changing its flat-band and band-edge potentials. Additionally, the EDT treatment could also increase carrier lifetime by suppressing unfavorable surface –OH and –O bonds (Fig. 5b). As a result, a considerably enhanced photocurrent of -31 mA cm^{-2} at -0.2 V vs. RHE of the EDT-treated GaN could be attained. Another study employed thioacetamide as an etching reagent to alleviate surface trap states and Fermi pinning in WO_3 photoanodes, which resulted in a decreased onset potential.⁶¹ Moreover, the influence of additional loading of the cocatalyst FeOOH layer and introducing the passivating layer Ga_2O_3 were evaluated. The onset potential values of different structures indicated that the interfacial properties of photoelectrodes could greatly affect their PEC performance.

These chemical modification approaches have been shown to be effective in altering the photophysical and electrochemical properties at the surface/interface of photoelectrodes by, for example, creating new chemical bonds. Both inorganic and

organic compounds are useful for enhancing metal-oxide as well as non-metal-oxide semiconductor photoelectrodes. Exploring the mechanism of these PEC enhancements can also promote our understanding of surface PEC water splitting reactions.

2.2.3 *In situ* ion exchange. Chemical treatments affect charge carrier behaviors of electrodes by altering surface states and surface physicochemical properties. From time to time, new materials/compositions are created onto pristine electrodes with chemical treatments, including the ion-exchange method. Recently, solution-based *in situ* ion exchange has been regarded as an effective approach to generate the heterostructure on pristine photoelectrodes. Note that this section does not include studies on the direct synthesis of photoelectrodes *via* ion exchange; for example, see ref. 62.

As reported by Chong *et al.*,⁶³ elemental Co was incorporated into a calcium hydroxyapatite structure ($\text{Ca}_{10}(\text{PO}_4)_6(\text{OH})_2$, Ca-

HAP) by immersing the Ca-HAP, which was coated onto Fe_2O_3 , in a $\text{Co}(\text{NO}_3)_2$ solution. The resultant Co-HAP-loaded Fe_2O_3 exhibited a significant enhancement (9.8 times) in photocurrent density, owing to the extraction of holes from Fe_2O_3 by PO_4^{3-} , active Co sites for surface hole transfer, arising from the 2D structure of $\text{Co}(\text{OH})_2$, the electrochemically active surface area (ECSA) was maximized and larger electrode/electrolyte interface was provided for reaction. The ECSA was increased from 0.051 mF cm^{-2} of Fe_2O_3 and 0.065 mF cm^{-2} of HAP/ Fe_2O_3 to 0.13 mF cm^{-2} of Co-HAP/ Fe_2O_3 . Chen *et al.* fabricated a $\text{BiVO}_4/\text{Bi}_2\text{S}_3$ heterojunction by immersing BiVO_4 -loaded conductive glass in a thiourea solution for a hydrothermal reaction.⁶⁴ By varying precursor sulfur, the convergence of Bi_2S_3 on BiVO_4 nanorods could be tuned. The highest photocurrent density of the $\text{BiVO}_4/\text{Bi}_2\text{S}_3$ heterojunction was 1.43 mA cm^{-2} at 1.23 V vs. RHE, compared to 0.25 mA cm^{-2} of bare BiVO_4 , because of the enhanced absorption by Bi_2S_3 and

Table 2 Various chemical modification approaches to treat photoelectrodes for PEC water splitting

Materials	Post-treatment	Photocurrent density ($\alpha \text{ mA cm}^{-2}$ at $\beta \text{ V}$ vs. γ ; δ times)	Ref.
Acid and alkaline treatments			
Fe_2O_3	Immersed in pure acetic acid for 5 min followed by annealing at 450°C for 30 min in air	1.2; 0.2; Ag/AgCl; 4.0	49
Ti-doped Fe_2O_3	Spin-coated with KOH, dried at 70°C for 12 h, and calcined at 400°C for 2 h in air	2.14; 1.6; RHE; 2.3	52
Ti-doped Fe_2O_3	Soaked in 1 M KOH at 80°C for 30 min	3.7; 1.5; RHE; 1.8	53
TiO_2	Hydrothermally heated in 0.1 M HNO_3 at 80°C for 1 h	2.8; 0.23; Ag/AgCl; 2.5	54
CaTaO_2N	0.2 g of CaTaO_2N added into 4 mL of aqua regia stirred for 20 s	0.025; 1.2; RHE; 4.0	55
ZrO_2	Soaked in 0.01 M HF acid for 1 h	-42.5; 0; RHE; 3.3	56
Ti-doped Fe_2O_3	Hydrothermally heated in 0.1 M HCl at 95°C for 1 h	2.0; 1.23; RHE; 1.3	1
Contact-induced surface alternations			
Fe_2TiO_5	Immersed in 0.2 M NH_4F with H_2O_2 at 60°C for 10 min, followed by annealing at 200°C for 20 min in air	0.4; 1.23; RHE; 2.2	10
$\text{Fe}_2\text{TiO}_5/\text{Fe}_2\text{O}_3$	Immersed in $\text{NH}_4\text{F}/\text{H}_2\text{O}_2$ solution at 60°C for 5 min	1.0; 1.0; RHE; 2.6	57
BiVO_4	Immersed in 0.5 M borate buffer (pH 9.3) for 12 h	3.5; 1.23; RHE; 2.2	19
Ti-doped Fe_2O_3	Immersed in 0.2 M Na_3PO_4 for 10 min, air-dried at 100°C for 1 h, and sintered at 250°C for 2 h in N_2	1.56; 1.23; RHE; 1.7	58
Ti-doped Fe_2O_3	Immersed in 0.5 M Na_2HPO_4 for 10 min, then annealed at 350°C for 1 h	2.56; 1.23; RHE; 1.7	59
Ti-doped Fe_2O_3	Hydrothermally heated in 10 mL methanol at 180°C for 10 h	2.2; 1.23; RHE; 1.5	1
GaN	Immersed in 1,2-ethanedithiol for 5 min	-31; -0.2; RHE; >31	13
WO_3	Immersed in 5 mg mL^{-1} thioacetamide at 80°C for 20 min	0.27; 1.2; RHE; 1.2	61
<i>In situ</i> ion exchange			
Ca-HAP ^a coated Fe_2O_3	Immersed in 50 mL of 0.01 M $\text{Co}(\text{NO}_3)_2$ solution at 40°C for 40 min	2.25; 1.23; RHE; 9.8	63
BiVO_4	Hydrothermally heated in 12–24 mg mL^{-1} of thiourea in aqueous solution at 170°C for 6 h, followed by washing and vacuum-drying at 200°C for 2 h	1.43; 1.23; RHE; 5.7	64
ZnO	Immersed in 0.32 M Na_2S aqueous solution, and heated at 60°C for 8 or 18 h in a water bath	0.60; 0.5; Ag/AgCl; 1.5	65
In_2S_3	Solvothermally heated in a mixture (15 mM $\text{Cu}(\text{NO}_3)_2$ and 0–45 mM thiourea in ethylene glycol) at 200°C for 12 h, followed by annealing at 400°C for 30 min in Ar	N/A	23
Cu_7S_4	Cu_7S_4 mixed with 4 mL of toluene and then swiftly adding to a well-mixed complex solution containing InCl_3 , followed by heating at 50°C for 2 h	0.06; 0.3; RHE; N/A	66

^a Ca-HAP: calcium hydroxyapatite.

the efficient charge transfer resulting from the type II heterojunction. Another study revealed the preparation of ZnO/ZnS core/shell nanorods by immersing ZnO nanorods in a Na₂S solution.⁶⁵ As a result of such chemical sulfidation treatment, both the surface roughness of the ZnO/ZnS and the crystallographic quality of the ZnO||ZnS interface were improved. The ZnO/ZnS heterojunction exhibited a photocurrent density of 0.60 mA cm⁻² at 0.5 V vs. Ag/AgCl, compared to 0.39 mA cm⁻² of bare ZnO photoanode. Feng *et al.* reported the synthesis of a p-

CuInS₂ or n-CuIn₅S₈ junction by solvothermally heating In₂S₃ in a Cu(NO₃)₂/thiourea solution.²³ By adjusting the amount of thiourea to control the cation exchange rate, the In₂S₃ could be controllably converted to various structures, including Cu_{1.81}S, CuInS₂/CuIn₅S₈, p-CuInS₂, and n-CuIn₅S₈ (Fig. 5c). With the addition of cocatalysts Pt and CoO_x on the p-CuInS₂ and n-CuIn₅S₈, respectively, self-biased PEC water splitting could be realized. Another study revealed that, by immersing Cu₇S₄ nanocrystals in an In-included solution, hollow

Table 3 Electrochemical treatments of photoelectrodes for improved PEC activity

Materials	Post-treatment	Photocurrent density (α mA cm ⁻² at β V vs. γ ; δ times)	Ref.
TiO ₂	Electrochemically reduced at a bias (-1.3, -1.5 or -1.8 V) for 5–20 min in 1 M KOH supporting electrolyte	0.53; 0.6; Ag/AgCl; 3.1	76
TiO ₂	Reduced at a bias voltage of -1.35 V in dark for 10–60 s in 1 M NaOH	0.70; 0.4; Ag/AgCl; 2.0	77
TiO ₂	Reduced at a potential of -0.5 V vs. RHE in 0.05 M H ₂ SO ₄ for 35–55 min	2.5; 1.23; RHE; 3.1	78
Ni,Si-codoped TiO ₂	Cathodically polarized at 5 V for 10 min in various electrolytes (0.5 mM H ₂ SO ₄ , 0.3 M Na ₂ SO ₄ or 0.1 M KOH)	2.41; 0; Ag/AgCl; 2.2	79
TiO ₂	Cathodically reduced at 4 V for 20 min in 0.1 M Na ₂ SO ₄	2.74; 0; Ag/AgCl; 3.4	81
TiO ₂	Reduced at a potential of -1.8 V vs. Ag/AgCl in 1 M NaOH for 10 s	2.4; 0; Ag/AgCl; 3.2	82
BiVO ₄	Cathodically reduced at a potential of -0.1 V vs. RHE in 1 M potassium borate electrolyte (pH 9.5)	2.5; 1.23; RHE; 10	4
Mo-doped BiVO ₄	Reduced at various potentials (-0.6, -0.8, -1.0 and -1.2 V vs. Ag/AgCl) for 5 min in 0.1 M Na ₂ SO ₄	4.3; 1.5; RHE; 4.3	83
BiVO ₄	Reduced at a potential of -0.8 V vs. Ag/AgCl in 0.5 M Na ₂ SO ₄ for 30 s	0.21; 1.0; Ag/AgCl; 3.5	82
Nb,Sn-codoped Fe ₂ O ₃	Electrochemically activated by a three-times cathodic scanning (from 1.0 to 0.2 V vs. RHE) followed by a three-times anodic scanning (from 1.0 to 2.2 V vs. RHE) in 1 M KOH	3.05; 1.23; RHE; 1.6	84
Ti-doped Fe ₂ O ₃	Reduced at a potential of -1.2 V vs. SCE for 1000 s in 1 M NaOH	0.62; 0.6; SCE; 1.93	85
Fe ₂ O ₃	Potentiostatically reduced at -1.5 to -0.8 V for 10 s, or cyclically reduced between -0.8 V and -1.5 V, followed by a stabilization process	N/A	15
WO ₃	Reduced at a potential of -0.8 V vs. Ag/AgCl in 0.5 M Na ₂ SO ₄ for 30 s followed by annealing at 300 °C for 5 min using a hotplate	0.53; 1.0; Ag/AgCl; 6.6	82
ZnO	Reduced at a potential of -1.2 V vs. Ag/AgCl in 0.5 M Na ₂ SO ₄ for 30 s	1.2; 1.0; Ag/AgCl; 1.3	82
GaN	Electrochemically etched at a voltage of 15 V for 10 min in an ethanol/hydrofluoric acid solution	4.0; 1.2; Ag/AgCl; 5.3	86
p-InP	Cathodically reduced at potentials from open-circuit potential to -0.06 V under illumination with intermittent passivation under dark condition	25; 0; RHE; 8.3	87

nanododecahedron-structured CuInS_2 nanocrystals could be generated.⁶⁶ As a result of the enhanced light-harvesting properties, the CuInS_2 photocathode showed an optimal photocurrent density of 0.06 mA cm^{-2} at 0.3 V vs. RHE .

These chemical modification approaches have been summarized in Table 2. It can be observed that various surface modification methods can substantially enhance the PEC activity of various photoelectrodes. Noticeably, beyond improving photoactivity, the chemical modification also is of crucial significance in aiding our understanding of the interaction among the surface structures of photoelectrodes, electrolyte composition, and light irradiation.

3. Electrochemical and irradiation-based treatments

3.1 Electrochemical treatments

Compared to chemical treatments, electrochemical treatments are not only simple and effective, but also can be performed in a controllable and reproducible manner. It is worth noting that the electrochemical reaction process could be precisely tuned and optimized by adjusting operation parameters. The electrochemical treatment methods have been summarized in Table 3.

As a representative of photoelectrodes, anatase and rutile TiO_2 photoanodes have been modified with various methods. Several fabrication approaches, such as hydrogenation,^{67–70} plasma treatments,^{71–74} and chemical reduction,^{70,75} have been confirmed to create self-doped Ti^{3+} -incorporated TiO_2 . In addition to these methods, electrochemical reduction as an effective approach has been studied to improve the photophysical and photoelectrochemical properties of TiO_2 . Song *et al.* prepared Ti^{3+} -self-doped TiO_2 by reducing it at cathodic potential.⁷⁶ Owing to the enhanced light absorption, improved conductivity and increased charge transfer rate, the self-doped TiO_2 exhibited an enhanced photocurrent density of 0.525 mA cm^{-2} at $0.6 \text{ V vs. Ag/AgCl}$, 3.1 times higher than that of pristine TiO_2 nanotubes. Significantly, another study demonstrated that the surface $\text{Ti}^{\text{III}}\text{O}(\text{OH})$ structure could be created with the assistance of electrochemical reduction at a bias more negative than the flat-band potential of TiO_2 .⁷⁷ It is interesting to note that, unlike previously reported reduced surface states, the electrochemically proton-doped TiO_2 photoanode exhibited an increased surface state density (*i.e.*, $\text{Ti}-\text{OH}$), which served to capture photogenerated electrons and suppress charge carrier recombination. The as-prepared TiO_2 exhibited a photocurrent density of 0.70 mA cm^{-2} at $0.4 \text{ V vs. Ag/AgCl}$, two times higher than that of bare TiO_2 . In addition, it was proved that electrochemical reduction could induce a type II structure, which enhances charge separation and transport⁷⁸ as well as creates self-doped Ti^{3+} accompanied by increasing the amount of O_{vac} in the TiO_2 photoanode.^{79–81} These studies validate that electrochemical treatments not only can affect the surface/interface properties of TiO_2 , but also improve its bulk attributes from time to time.

Wang *et al.* reported the electrochemical reduction of various metal oxide photoanodes, including WO_3 , TiO_2 , BiVO_4 , and

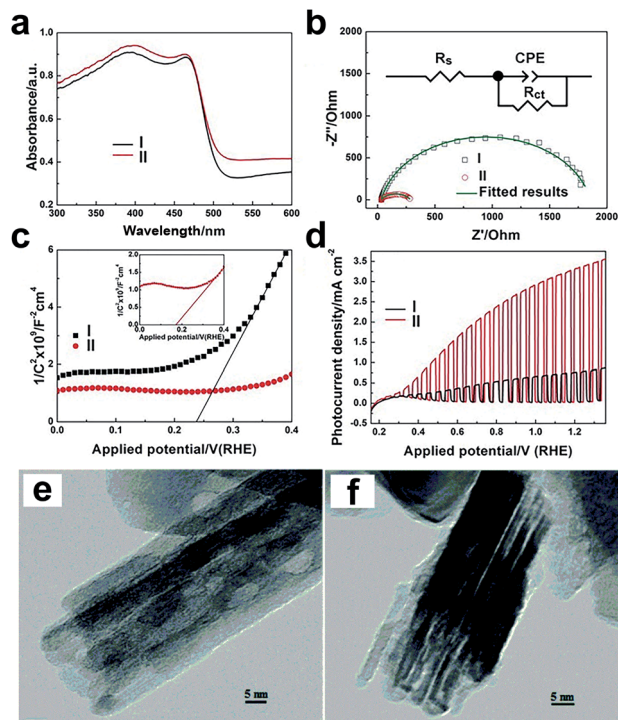


Fig. 6 (a) UV-visible spectra, (b) electrochemical impedance spectra, (c) Mott–Schottky curves, and (d) chopped J – V curves of bare BiVO_4 (I) and electrochemically reduced BiVO_4 (II) in 1 M KPi buffer with $0.2 \text{ M Na}_2\text{SO}_3$ ($\text{pH } 9.5$).⁴ Reprinted with permission from ref. 4, copyright 2017 Wiley-VCH Verlag GmbH & Co. KGaA, Weinheim. (e and f) TEM images for Fe_2O_3 nanorods (e) before and (f) after electrochemical reduction, showing more individual nanowires.¹⁵ Modified with permission from ref. 15, copyright 2017 the Owner Societies.

ZnO .⁸² With the electrochemical treatments, O_{vac} could be controllably introduced in these photoanodes. As a result of the improved charge separation and injection properties, all these electrochemically treated photoanodes exhibited substantially improved PEC performance. Another study comprehensively explored the effects of electrochemical reduction on the photoactivity of BiVO_4 photoanodes.⁴ After electrochemical reduction at 0.1 V vs. RHE for only 150 s , the as-treated BiVO_4 exhibited a 10-fold increase in photocurrent density. The significantly enhanced PEC activity was attributed to the generation of O_{vac} , which substantially facilitated bulk and surface charge separation (Fig. 6a–d). In another study, by imposing Mo-doped BiVO_4 photoanodes with various bias potentials, the contrary roles of as-created O_{vac} and quasioxygen vacancies were explored.⁸³ It was revealed that the O_{vac} generated at a bias of $-1.2 \text{ V vs. Ag/AgCl}$ were detrimental to PEC performance. In comparison, the quasioxygen vacancies formed at a bias of $-0.8 \text{ V vs. Ag/AgCl}$ could increase charge carrier density and thus improve the photocurrent density to 4.3 mA cm^{-2} at 1.5 V vs. RHE , 4.3 times higher than that of untreated BiVO_4 photoanodes.

For Fe_2O_3 photoanodes, the passivation of an Nb- and Sn-doped Fe_2O_3 photoanode using an electrochemical activation method was realized.⁸⁴ After cathodic scanning three times, followed by anodic scanning three times, the as-treated Fe_2O_3

exhibited a photocurrent density of 3.05 mA cm^{-2} at 1.23 V vs. RHE , which is 1.6 times higher than that of bare Fe_2O_3 . The enhanced performance could be attributed to the etching of surface dangling defects, the enriched Nb–O and Sn–O bonds that passivated the surface states, and the creation of Fe^{2+} and O_{vac} , which improved conductivity. In spite of the effectiveness of employing electrochemical reduction treatment to boost Fe_2O_3 , the fundamental mechanism has not been well-understood. In view of this, Zhang *et al.* reported their work in which they constructed a new charge carrier dynamics model to explore surface-state mediated charge transfer and recombination.⁸⁵ Their results indicated that a new type of surface state, generated by the electrochemical reduction of Fe_2O_3 . The new surface state is peaked at $\sim 0.1 V_{\text{SCE}}$ which is $0.05 V_{\text{SCE}}$ lower than the bare Fe_2O_3 . Such shift in surface state favours the overlapping of unoccupied surface state of electrodes and filled levels of the redox couple, leading to increased charge transfer rate constant and enhanced surface water oxidation process. Additionally, the negatively shifted flat-band potential resulted in reduced electron density, leading to the reduction of the charge recombination rate. By contrast, the report by Cibrev *et al.* pointed out that the enhanced PEC performance of electrochemically reduced Fe_2O_3 , an eight-fold increase in transient photocurrent, should be primarily ascribed to the n-type doping (*e.g.*, the generation of Fe^{2+} or other polaron species) as well as to the change in film morphology (Fig. 6e and f).¹⁵

In addition to metal oxide photoelectrodes, III–V semiconductors can also be tailored using electrochemical treatments, and the reports of n-GaN and p-InP are two examples.^{86–88} Cao *et al.* reported the electrochemical etching of GaN-based thin films in an ethanol/hydrofluoric acid solution, with the intention of peeling off mesoporous InGaN/GaN layers.⁸⁶ After transferring the free-standing GaN-based layers on the n-Si substrate, the as-prepared photoanode exhibited a low turn-on voltage and high efficiency, which could be attributed to the increase of surface area and the relaxation of stress. The etched sample was reported with specific area (S_{BET}) with $3.97 \text{ m}^2 \text{ g}^{-1}$. In another study by Goryachev *et al.*,⁸⁷ the combination of cathodic scanning with open circuit/dark resting for the treatment of p-InP photocathodes allowed a 27-fold increase in photocurrent density. Moreover, with an online electrochemical mass spectrometry technique, the influence of the employed electrolytes (*i.e.*, H_2SO_4 or HCl) on the surface passivation was examined. It appeared that InO_x and InPO_x at the material surface could be generated when using H_2SO_4 as an electrolyte, while insoluble InCl was formed when using HCl as an electrolyte. The results indicated the need to evaluate faradaic efficiencies of reactions (*e.g.*, HER and OER) using chemical-specific techniques.

3.2 Irradiation-based treatments

Light/irradiation treatments are effective for modifying photoelectrodes, such as BiVO_4 and Fe_2O_3 . This facile method exhibits simplicity and effectiveness and can avoid extra complex material processing steps in the optimization of practical PEC water splitting systems.

Irradiation treatments for BiVO_4 photoanodes have been presented. For instance, after exposure to UV radiation in the air for 20 h, the surface of BiVO_4 could be cured.⁸⁹ UV light-induced passivation of surface states (*e.g.*, dangling oxygen) reduced the charge trapping possibility, as reflected by an increased charge carrier density. Additionally, the cathodic shift of flat-band potential also contributed to the wide separation of quasi-Fermi levels of electrons and holes, which benefited charge separation. As a result, the as-treated BiVO_4 exhibited a photocurrent density of 1.1 mA cm^{-2} at 1.23 V vs. RHE , 2.2 times higher than that of bare BiVO_4 , accompanied by a remarkable shift of onset potential (400 mV). Likewise, illuminating BiVO_4 in a 0.1 M KPi buffer with AM 1.5 G light under an open-circuit condition,⁵ known as photocharging, could induce a 4.4-fold increase in photocurrent density (3.3 mA cm^{-2} at 1.23 V vs. RHE for as-illuminated BiVO_4) and a cathodic shift of onset potential (300 mV). It was shown that the light-induced passivation of surface states could result in an increased photovoltage by eliminating detrimental Fermi level pinning (Fig. 7a and b), responsible for the enhanced PEC performance. Their follow-up study further revealed that the pH of exposed electrolytes has a great influence on such photocharging effects.⁹ Illuminating BiVO_4 photoanodes at pH 10 under open-circuit conditions achieved a high photocurrent density of 4.3 mA cm^{-2} at 1.23 V vs. RHE , while the photocurrent density of processed BiVO_4 photoanodes at pH 4 remained unchanged, as 1.0 mA cm^{-2} at 1.23 V vs. RHE . It has been suggested that the formation of

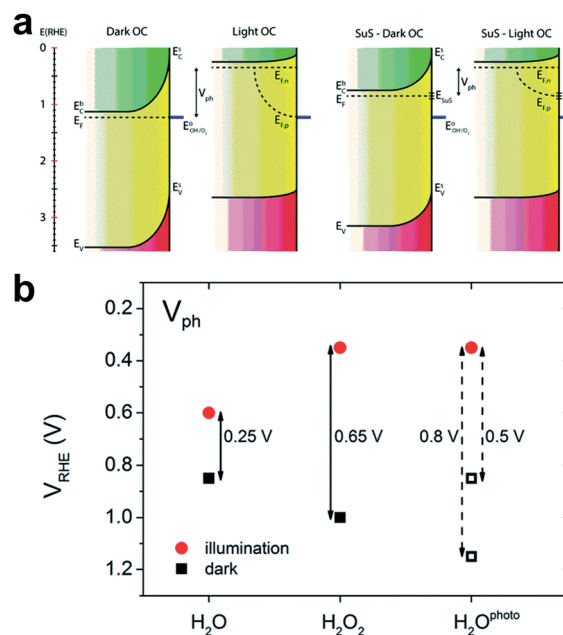


Fig. 7 (a) Electronic band diagrams for BiVO_4 under open-circuit conditions: dark, without illumination; light, with illumination; SuS, with photocharging-induced surface states. (b) Equilibrium potentials and photovoltage values of BiVO_4 photoanodes under open-circuit conditions. Untreated sample in 0.1 M KPi electrolyte (H_2O) or a hole scavenger (H_2O_2), or photocharged sample in 0.1 M KPi electrolyte ($\text{H}_2\text{O}_{\text{photo}}$).⁵ Reprinted with permission from ref. 5, copyright 2016 The Royal Society of Chemistry.

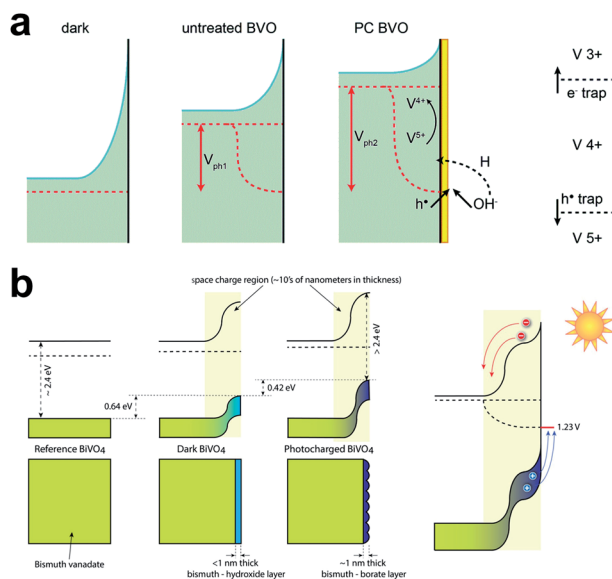


Fig. 8 (a) Band diagrams of BiVO₄ in the dark and under illumination before and after photocharging treatment, including the simplified photocharging mechanism model.⁹ Reprinted with permission from ref. 9, copyright 2017 The Royal Society of Chemistry. (b) Effect of photocharging on the bandgap region and the Fermi level of BiVO₄. Hydroxide (dark sample) and bismuth borate (photocharged sample) surface layers have a valence band closer to the Fermi level, introducing band bending at the surface. The band bending directs electrons toward the bulk of BiVO₄, leading to a reduced electron concentration in the space charge region for photocharged BiVO₄. The effect of photocharging on a BiVO₄ photoanode in contact with an electrolyte under illumination is shown. The additional band bending improves the charge separation, leading to the unrivaled PEC properties of the photocharged BiVO₄.²² Reprinted with permission from ref. 22, copyright 2019 American Chemical Society.

active water oxidation intermediates and/or the change of surface chemistry, which enhanced the electrocatalysis reaction (Fig. 8a), should be the reasons for the boosted PEC water splitting performance. Firet *et al.* further investigated the surface chemistry of BiVO₄ during photocharging.²² Notably, by employing ambient-pressure X-ray Raman scattering spectroscopy as a tool, the researchers demonstrated that a BiVO₄ surface could adsorb electrolyte anion species, generating a bismuth borate layer under illumination. The light-induced heterojunction structure could lead to additional band bend in the space charge region, thus resulting in an improved charge separation efficiency and a suppressed charge recombination rate (Fig. 8b). Another study particularly employed intensity-modulated photocurrent spectroscopy (IMPS) to investigate the impact of photocharging on both bulk and surface properties of BiVO₄.⁹⁰ With this technique, the 1.91-fold increase in the photocurrent density at 1.2 V vs. RHE has been ascribed to a 45% improvement in surface charge transfer efficiency as well as to a 46% improvement in bulk charge separation efficiency.

Additionally, two examples are presented to demonstrate the importance of an immersion solution during the photocharging process.^{91–93} As reported by Feng *et al.*, immersing BiVO₄

photoanodes in a Na₂SO₃/KBI solution for only 10 min under illumination could induce considerable amounts of surface O_{vac} at the surfaces.⁹¹ Because these surface O_{vac} could contribute to the formation of interband states, as indicated by DFT calculations, improved charge separation efficiency at the BiVO₄-||electrolyte interface was observed. As a result, the photoetched BiVO₄ exhibited a photocurrent density of 3.55 mA cm⁻² at 0.6 V vs. RHE, two times higher than that of untreated BiVO₄. In a similar way, Yin *et al.* reported the use of sulfite to treat BiVO₄ photoanodes under illumination.⁹³ It was revealed that the photogenerated holes could be consumed by sulfite ions that were oxidized to sulfate ions, while the remaining electrons could reduce V⁵⁺ to V⁴⁺ and thus indirectly create O_{vac} in BiVO₄ photoanodes, rather than directly invoking the formation of O_{vac} by reaction between holes and lattice oxygen. Remarkably, the self-reduced BiVO₄ exhibited a photocurrent density of 3.18 mA cm⁻² at 1.23 V vs. RHE, compared to 1.44 mA cm⁻² of the bare one.

In addition to BiVO₄, other photoelectrodes, such as Fe₂O₃, WO₃, CuWO₄, and TiO₂, can also be distinct after irradiation treatments. Xie *et al.* investigated the influence of stability tests under long-term illumination on the PEC performance of Ti-doped Fe₂O₃.⁶ Their results indicated an improvement in photocurrent density and a cathodic shift of onset potential after illumination for 12–70 h. The enhanced photoactivity was attributed to the generation of FeOOH, which acted as a cocatalyst to facilitate hole transfer (Fig. 9a). In spite of this, in contrast to the generation of Fe²⁺, Deng *et al.* revealed that high-valence Fe(IV), created by illumination for 30–150 min at a bias of 1.23 V vs. RHE and detected by O K-edge X-ray absorption spectroscopy (XAS) (Fig. 9b), should be responsible for the

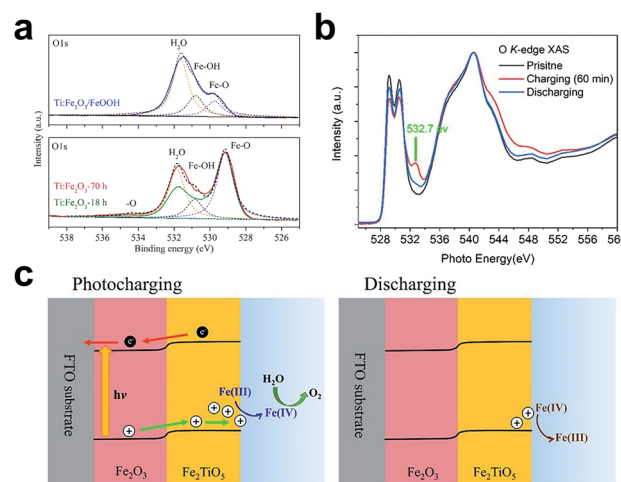


Fig. 9 (a) XPS O 1s spectra of Ti-doped Fe₂O₃ photoanodes after 18 and 70 h stability testing and photoelectrochemically deposited FeOOH on Ti-doped Fe₂O₃.⁶ Reprinted with permission from ref. 6, copyright 2018 American Chemical Society. (b) O K-edge XAS spectra of pristine Fe₂TiO₅/Fe₂O₃ film (black curve), a photocharged Fe₂TiO₅/Fe₂O₃ film for 60 min (red curve), and a discharged Fe₂TiO₅/Fe₂O₃ film for 10 min (blue curve), respectively. (c) Schematic illustration of photocharging and discharging of Fe₂TiO₅/Fe₂O₃.²⁰ Modified with permission from ref. 20, copyright 2018 American Chemical Society.

increased photocurrent density.²⁰ Importantly, the Fe(IV) species could restore to Fe(III) at light switch-off, pointing out the importance of exploring effective methods to preserve the created advantageous surface structures (Fig. 9c).

Li *et al.* examined the impact of UV light exposure on the PEC performance of WO₃ photoanodes.⁹⁴ After UV irradiation in the air for 4 h, the UV-radiated WO₃ exhibited a photocurrent density of 0.69 mA cm⁻² at 1.23 V vs. RHE, 1.3 times higher than that of untreated WO₃. Different from the occurrence of surface chemistry changes in photoelectrodes such as BiVO₄ (the formation of bismuth borate)²² and Fe₂O₃ (the generation of FeOOH or Fe(IV)),^{6,20} this work revealed that the light exposure only led to a high film porosity and thus a high specific surface area, which is responsible for the enhancement in photoactivity of WO₃. The surface area was not measured, the increment of surface area was determined by the porous formation on SEM images. In another work, Breuhaus-Alvarez *et al.* analyzed the interaction between the photochromism effect and PEC properties of WO₃ photoanodes.⁹⁵ It was demonstrated that the PEC decay of WO₃ should be related to the change of surface chemistry instead of to the dissolution of WO₃ itself, because the PEC performance of WO₃ photoelectrodes could be fully recovered by illumination under the open-circuit condition in

the electrolyte. The report highlighted the importance of exploring the influence of intercalation/deintercalation behaviors on photoelectrodes.

Photocharging treatments could also enhance the photoactivity of CuWO₄.⁹⁶ Prolonged exposure to 1 sun illumination for 15 h doubled the photocurrent density of CuWO₄ at 1.23 V vs. RHE. The formation of a heterostructured copper borate layer at the CuWO₄ surface, which facilitated charge separation and suppressed charge recombination, should be the reason for the enhanced photoactivity. This work, together with other photocharging studies, suggests a complex metal oxide electrode|electrolyte interface,^{6,22} demanding more efforts to study interfacial properties for realizing practical PEC water splitting. Additionally, pulsed laser irradiation could also be useful for the treatment of photoelectrodes, such as TiO₂ nanotubes.⁹⁷ The as-optimized TiO₂ photoanode exhibited a 1.6-fold increase in photocurrent density, which was ascribed to an increased charge carrier donor density and reduced deep trapping states.

These irradiation-based treatments are summarized in Table 4. It can be seen that the surroundings of the photoelectrodes (*e.g.*, air or electrolyte of different compositions) during the irradiation treatments have a significant influence on the resultant PEC responses. This indicates that beneficial

Table 4 Various irradiation-based treatments of photoelectrodes for PEC applications

Materials	Post-treatment	Photocurrent density (α mA cm ⁻² at β V vs. γ ; δ times)	Ref.
BiVO ₄	Exposed to UV radiation (185 and 254 nm, 10 mW cm ⁻²) in the air for 20 h	1.1; 1.2; RHE; 2.2	89
BiVO ₄	Exposed to AM 1.5 light in a 0.1 M phosphate buffer (pH 7.2) under open-circuit condition for 10 h	3.3; 1.23; RHE; 4.1	5
BiVO ₄	Exposed to AM 1.5 light in a 0.1 M phosphate-borate-acetate buffer (pH 4, 7 or 10) under open-circuit condition for 10 h	4.3; 1.23; RHE; 3.9	9
BiVO ₄	Illuminated by AM 1.5 light (1 sun) in a 0.5 M phosphate buffer under open-circuit condition for 3 h	1.0; 1.23; RHE; 2.0	90
BiVO ₄	Illuminated by AM 1.5 G light in a 1 M potassium borate containing 0.2 M Na ₂ SO ₃ for 10 min without external bias	3.55 ^a ; 0.6; RHE; 2.0	91
BiVO ₄	Irradiated by AM 1.5 G light in a 0.2 M Na ₂ SO ₃ solution for 40 min	3.18; 1.23; RHE; 2.2	93
Ti-doped Fe ₂ O ₃	Exposed to 100 mW cm ⁻² light in 1 M NaOH at 1.23 V vs. RHE for 70 h	0.32; 1.23; RHE; 1.2	6
Fe ₂ TiO ₅ /Fe ₂ O ₃	Exposed to 1 sun light in 1 M NaOH at 1.23 V vs. RHE for 30–150 min	2.02; 1.23; RHE; 1.2	20
WO ₃	Exposed to UV radiation (185 and 254 nm, 10 mW cm ⁻²) in air for 4 h	0.69; 1.23; RHE; 1.3	94
CuWO ₄	Exposed to AM 1.5 light in a 0.3 M borate buffer with 0.1 M NaClO ₄ (pH 7.5) for 15 h under open-circuit condition	0.06; 1.23; RHE; 2.0	96
TiO ₂	Irradiated by a 248 nm pulsed laser when immersing in DI water for 60 s	0.36; 1.23; RHE; 1.6	97

^a Measured in 1 M potassium borate buffer (pH 9.0) containing 0.2 M Na₂SO₃.

structures could be generated as the photochemical reactions transpire. On the flip side, it should be acknowledged that, in general, these structures may not be so stable when standing still in the electrolyte under dark/illumination conditions. Exploring advanced techniques to scrutinize the formation and diminishing of the structures and seeking effective methods by which to preserve them are therefore of crucial importance.

4. Post-annealing treatments

Post-annealing modification is always an effective method for changing the surface and bulk properties of photoelectrodes. In this section, gas-based annealing under various atmospheres, such as H_2 ,^{7,98–107} NH_3 ,^{18,108–114} N_2 ,^{115–117} Ar ,^{118,119} CO ,¹²⁰ O_2 ,^{24,121,122} and $(NH_4)_2S$,¹²³ and other unique annealing techniques including solid-based annealing, employing S ,¹²⁴ Mg ,¹⁶ and Zn ,^{125,126} and flame annealing^{11,127} as well as vacuum annealing^{21,128} have been introduced. It should be noted that this section does not include studies of the two-step annealing process, for instance, dip-coating followed by annealing,¹²⁹ to avoid complexity and confusion.

4.1 Gas annealing

4.1.1 Hydrogen annealing. Since the report of Chen *et al.* in 2011,¹³⁰ hydrogen annealing, also called hydrogenation, has been extensively explored for the treatment of TiO_2 . In general, the enhanced photoactivity of hydrogenated TiO_2 can be ascribed to extra visible light absorption as well as to the optimized surface structures for reducing charge recombination

and enhancing charge transfer.^{131–136} By contrast, Mohajernia *et al.* reported the annealing of TiO_2 in the Ar/H_2 atmosphere.¹⁰⁵ They found that the enhanced PEC performance should be dominantly attributed to strongly improved conductivity (*i.e.*, semimetallic properties) as a result of the formation of O_{vac} and Ti^{3+} , and slightly due to the enhancement in light absorption. Another study also reported the high conductivity of anatase TiO_2 post-annealed in the Ar/H_2 atmosphere.¹⁰⁶

High-temperature annealing at 650–850 °C not only induced the creation of O_{vac} and Ti^{3+} species but also rendered the generation of various phases, including Ti_2O_3 , TiO , Ti_4O_7 , and rutile TiO_2 . Owing to limited interfacial charge recombination and a two-order enhancement in charge carrier density, the as-prepared TiO_2 photoanode exhibited a 2.4-fold increase in photocurrent density. Recently, Liu *et al.* compared the stability of hydrogenated and cathodically reduced TiO_2 photoanodes.¹⁰⁷ It was revealed that black TiO_2 , resulting from hydrogenation treatment, was of high stability during an electrochemical oxidation test. In comparison, the same experiment could easily degenerate cathodically reduced TiO_2 . The study of Liu *et al.* proves the reliability of post-annealing treatments.

In addition to TiO_2 , photoelectrodes such as WO_3 , $SrTiO_3$, and $ZnFe_2O_4$ could be hydrogenated as well. Zhang *et al.* revealed that surface O_{vac} in WO_3 , created by hydrogenation, could serve as recombination centers for photogenerated charge carriers.⁷ Interestingly, an ozone treatment was employed to cure these surface defects while reserving beneficial bulk O_{vac} (Fig. 10a). The treatments eventually resulted in a cathodic shift of 0.15 V and a photocurrent density of 2.25 mA cm^{-2} (Fig. 10b). The introduction of O_{vac} for intrinsic doping

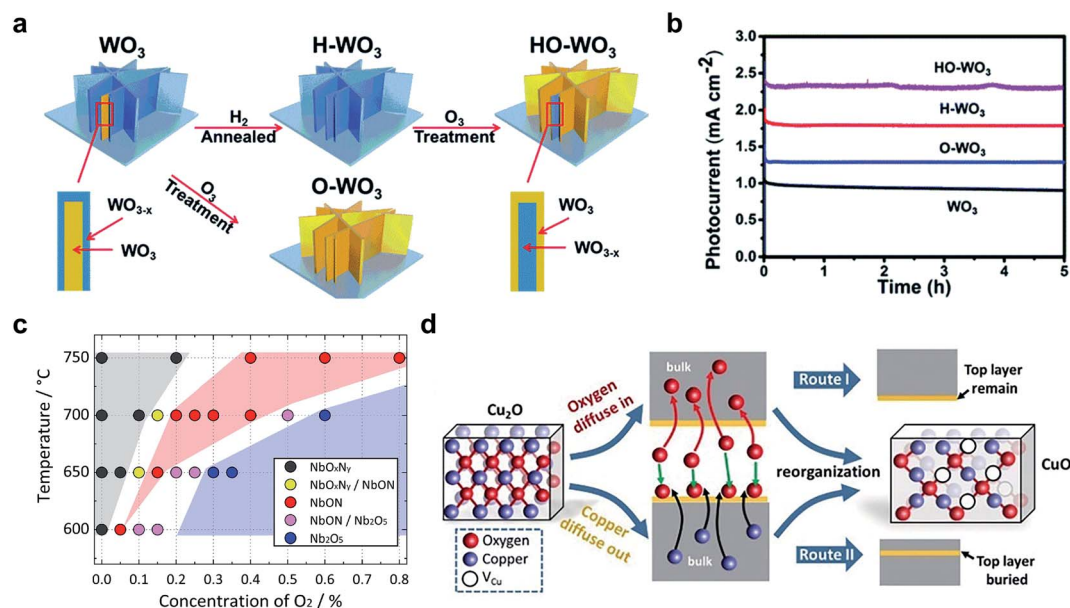


Fig. 10 (a) Schematic of the synthesis process of H_2 -annealed WO_3 ($H-WO_3$), H_2 -annealed WO_3 followed by ozone treatment ($HO-WO_3$), and only ozone-treated WO_3 ($O-WO_3$), and (b) $J-t$ curves of bare WO_3 , $H-WO_3$, $HO-WO_3$, and $O-WO_3$ photoanodes under AM 1.5 G at 1.23 V vs. RHE.⁷ Reprinted with permission from ref. 7, copyright 2018 The Royal Society of Chemistry. (c) The crystal phase of generated nitrated products from Nb_2O_5 depends on O_2 concentration and reaction temperature in the nitrogen annealing process.¹⁸ Reprinted with permission from ref. 18, copyright 2018 Elsevier Ltd. (d) Schematic illustration of two routes for the formation of CuO from Cu_2O .²⁴ Reprinted with permission from ref. 24, copyright 2019 Wiley-VCH Verlag GmbH & Co. KGaA, Weinheim.

could enhance the PEC activity of photoelectrodes. Also, hydrogen intercalation could provide an opportunity to tune the absorption characteristics and charge carrier behaviors in photoelectrodes. In the study by Gu *et al.*, the synergetic effects between O_{vac} and intercalated hydrogen in WO_3 were investigated.¹⁰¹ O_{vac} was generated by hydrogenation treatment, while a subsequent two-step photoelectrochemical treatment was employed to realize hydrogen intercalation. Owing to boosted spatial charge separation efficiency resulting from oxygen-deficient defects and hydrogen-intercalated structures, the as-treated WO_3 photoanode exhibited a high photocurrent density of 2.94 mA cm^{-2} at 1.23 V vs. RHE . Hydrogenation could also drive the conversion of the WO_3 semiconductor to a semi-metallic compound,¹⁰² similar to that in the report of TiO_2 .¹⁰⁶ The creation of O_{vac} , as a result of the hydrogenation, not only increased conductivity but also narrowed the band structure of the photoanode, allowing the absorption of infrared light. The as-produced WO_3 exhibited a photocurrent density of 0.21 mA cm^{-2} at $1.2 \text{ V vs. Ag/AgCl}$ under infrared light and a dark current density of 0.14 mA cm^{-2} . Yan *et al.* investigated the synergistic effect of combining heterojunction with hydrogenation.⁹⁹ The as-prepared hydrogenated $SrTiO_3/TiO_2$ heterojunction exhibited a photocurrent density of 0.48 mA cm^{-2} at 1.0 V vs. SCE , 3.0 times of that of hydrogenated TiO_2 and 1.5 times of that of bare $SrTiO_3/TiO_2$. The enhanced PEC performance was due to the improved light absorption as well as to the increased charge carrier density. Kim *et al.* presented a series of strategies to process $ZnFe_2O_4$ photoanodes.¹⁰⁰ Hydrogen annealing at $200 \text{ }^\circ\text{C}$ for 2 h, as one of these strategies, improved the photocurrent density from 0.22 mA cm^{-2} to 0.79 mA cm^{-2} at 1.23 V vs. RHE , owing to the generated O_{vac} , which increased majority carrier density.

As summarized in Table 5, hydrogen annealing is an effective and robust approach for modifying various photoelectrodes. It is widely accepted that this treatment can easily introduce surface and/or bulk O_{vac} in photo-responsive materials, benefiting charge transport and transfer.

4.1.2 Annealing in other gases. Ammonia (NH_3) is a useful chemical for realizing the nitridation of various photoelectrodes, such as $Ta_2O_xN_y$,¹⁰⁹ $NbON$,¹⁸ $SrNbO_2N$,¹⁰⁸ Ta_3N_5 (ref. 113) and TiO_2 .¹¹⁴ Zhang *et al.* investigated the roles of internal electric fields and charge transport behaviors in type II $Ta_2O_xN_y/TiO_2$ heterostructures obtained by the ammonization of Ta_2O_5/TiO_2 .¹⁰⁹ The as-prepared $Ta_2O_xN_y/TiO_2$ was endowed with improved hydrophilicity, decreased overpotential, as well as enhanced bulk charge separation and transport properties. As a result, the as-prepared photoanode exhibited a photocurrent density of 1.32 mA cm^{-2} at 1.23 V vs. RHE , 12 times and 4.3 times higher than that of bare TiO_2 and Ta_2O_5/TiO_2 photoelectrodes, respectively. Another study explored the role of small amounts of oxygen mixed in ammonia.¹⁸ Interestingly, $NbON$ (of Nb^{5+}) could be generated with the presence of $\sim 0.05\text{--}0.40\%$ oxygen during the nitridation of Nb_2O_5 (Nb^{5+}). The mixed oxygen avoided the generation of unfavorable NbO_xN_y (Nb^{2+} and Nb^{3+}) resulting from the reduction of Nb, proving the relevance between oxygen and the synthesis of oxynitrides (Fig. 10c). The study of Tamura *et al.* provided a special path for

realizing the nitridation of photoelectrodes. Kodera *et al.* examined and compared the nitridation mechanisms of $Sr_2Nb_2O_7$ and $SrNbO_3$ to $SrNbO_2N$.¹⁰⁸ It was shown that the reaction between $Sr_2Nb_2O_7$ and NH_3 involved both the introduction of nitrogen and the extraction of oxygen, leading to lattice shrinkage and thus to a porous structure. In comparison, the nitridation of $SrNbO_3$ only introduced the N element into the photoelectrode, resulting in lattice expansion and phase separation. In another work, Ta_3N_5 photoanodes were prepared from Ta foil by an electrochemical anodization method followed by post-annealing in a N_2/NH_3 gas mixture.¹¹³ Annealing at a temperature of $1000 \text{ }^\circ\text{C}$ resulted in the highest photocurrent density, due to high crystallinity, broad light absorption, as well as the formation of a conductive interlayer between substrates. In addition to nitridation, ammonia annealing has the ability to motivate the chemical reduction of photoelectrodes without the introduction of elemental nitrogen. For example, Xu *et al.* demonstrated that the post-annealing of TiO_2 in Ar/NH_3 could introduce O_{vac} and Ti^{3+} species in the photoanode without concurrent nitrogen doping,¹¹⁴ similar to the reported WO_{3-x} by Liu *et al.*¹³⁷ As a consequence of enhanced visible light absorption, increased charge carrier density and reduced flat-band potential, the as-obtained TiO_2 exhibited a four-fold enhancement in photocurrent density. The work of Xu *et al.* clarified the contribution and roles of exclusive O_{vac} without substitutional N dopants.

Various gases, such as CO ,¹²⁰ N_2 ,¹¹⁵ Ar ,^{118,119} and O_2 ,^{24,121} can be used for efficient post-synthetic annealing treatments. Zhang *et al.* investigated H_2 or CO as an annealing gas for the treatment of $BiVO_4$.¹²⁰ The H_2 annealing primarily introduced hydrogen donors in $BiVO_4$, which improved minority carrier (*i.e.*, holes) transport. In contrast, CO annealing exclusively induced O_{vac} , resulting in enhanced majority carrier (*i.e.*, electrons) transport. Owing to the decreased polaron hopping barrier, the conductivity of the CO -annealed photoanode was improved, thus promoting PEC responses. It is extensively recognized that broadening light absorption and improving charge separation efficiency should be the main contributions of O_{vac} . In spite of this, Lv *et al.* especially explored the role of O_{vac} in charge injection.¹¹⁵ They introduced O_{vac} in TiO_2 by a one-step annealing treatment. Both the theoretical and experimental studies proved that O_{vac} chiefly increased electrochemically active surface area and reactivity, which accelerated hole transfer and reduced overpotential, finally resulting in a 5.8-fold increase in photocurrent density. Seo *et al.* explored a new route by which to fabricate high-performance $BaNbO_2N$ photoanodes,^{118,119} which included moderate nitridation followed by post-annealing in Ar flow. The as-prepared Ar -annealed $BaNbO_2N$ exhibited a 5-fold enhancement in PEC performance, which should be ascribed to increased crystallinity and reduced surface defect density. In comparison, post-annealing $BaNbO_2N$ in NH_3 could increase crystallinity but unfavorably increased the number of surface defects. Wang *et al.* annealed Cu_2O photocathodes in pure oxygen to generate copper vacancies in CuO (Fig. 10d).²⁴ Both theoretical and experimental results indicated the formation of metal vacancies in CuO . As a result of enhanced majority carrier density and

Table 5 Various post-annealing treatments for photoelectrodes

Materials	Post-treatment	Photocurrent density (α mA cm ⁻² at β V vs. γ ; δ times)	Ref.
Hydrogen annealing			
TiO ₂	Annealed in H ₂ (10% in Ar) at 450–550 °C	0.6; 1.2; RHE; 5.5	105
TiO ₂	Annealed in H ₂ (5% in Ar) at 650–850 °C for 5–120 min	0.54; 1.23; RHE; 2.4	106
WO ₃	Annealed in H ₂ (60 sccm) at 350 °C for 10–60 min, followed by O ₃ treatment (40 sccm) at 100 °C for 10–60 min	2.25; 1.23; RHE; 2.0	7
WO ₃	Annealed in H ₂ (5% in Ar, 100 mL min ⁻¹) at 400 °C for 2 h, followed by electrochemically oxidized at 1.5 V vs. Ag/AgCl under light for 4 h, and then reduced at -0.5 V vs. Ag/AgCl under dark for 30 s	2.94; 1.23; RHE; 2.3	101
WO ₃	Annealed in pure H ₂ (20 mL min ⁻¹) at 250–450 °C for 20–360 min	0.21 ^a ; 1.2; Ag/AgCl; N/A	102
SrTiO ₃ /TiO ₂	Annealed in pure H ₂ at 300–400 °C for 30 or 60 min	0.48; 1.0; SCE; 1.5	99
ZnFe ₂ O ₄	Annealed under H ₂ atmosphere at 200 °C for 2 h	0.79; 1.23; RHE; 3.6	100
Ammonia annealing			
Ta ₂ O ₅ /TiO ₂	Annealed in NH ₃ (100 mL min ⁻¹) at 500 °C for 30 min	1.32; 1.23; RHE; 4.3	109
Nb ₂ O ₅	Annealed in NH ₃ /O ₂ /N ₂ (20% of NH ₃ and 0–0.80% of O ₂ , 500 sccm) at 600–750 °C for 1 h	0.6 ^b ; 1.23; RHE; N/A	18
Sr ₂ Nb ₂ O ₇	0.5 g of Sr ₂ Nb ₂ O ₇ heated under NH ₃ (250 mL min ⁻¹) at 900 °C for 1–40 h	N/A	108
SrNbO ₃	0.5 g of SrNbO ₃ heated under NH ₃ (250 mL min ⁻¹) at 900 °C for 1–40 h	N/A	108
TaO _x	Annealed in NH ₃ (10% in N ₂ , 40 mL min ⁻¹) at 600–1000 °C for 3 h	0.25; 1.23; RHE; N/A	113
TiO ₂	Annealed in NH ₃ (100 sccm) at 450 °C for 7.5 min followed by annealing in Ar at 450 °C for 1–4 h	0.93; 1.23; RHE; 4.0	114
Annealing in other gases			
BiVO ₄	Annealed in pure CO (20 sccm) at 300 °C for 20 min	2.25; 1.23; RHE; 1.5	120
TiO ₂	Annealed under N ₂ atmosphere at 800 °C for 2 h	1.02; 1.23; RHE; 5.8	115
BaNbO ₂ N	Annealed in pure Ar (100 mL min ⁻¹) at 400–800 °C for 10–120 min	5.0; 1.23; RHE; 5.0	118
Cu ₂ O	Annealed in N ₂ /O ₂ mixed gas (200 mL min ⁻¹ , ratio changed from 0 to 9) at 450 °C for 2 h	-1.8; 0.1; RHE; 2.0	24
WO ₃	Annealed in controlled oxygen pressure (95 mTorr) at 500 °C for 200–600 s	1.81; 1.23; RHE; 2.0	121
Solid-based annealing			
Fe ₂ O ₃	Annealed in the air at 400 °C for 20 min with upstream S powder	1.42; 1.23; RHE; 2.45	124
BiVO ₄	Annealed in N ₂ at 370 °C for 2 h and then in air at 450 °C for 15 min with PVDF ^c aside	0.28; 1.23; RHE; 1.4	8
TiO ₂	Ground with Mg powder, sealed and annealed at 500 °C for 10 h, followed by washing, filtering and drying	3.0; 1.0; RHE; 5.0	16
Ni-doped TiO ₂	Annealed in Ar at 500 °C for 4 h with upstream Zn particles heated at 700 °C	2.06; 0; Ag/AgCl; 2.2	126
Si-doped TiO ₂	Annealed in Ar at 500 °C for 4 h with upstream Zn particles heated at 700 °C	1.78; 0; Ag/AgCl; 2.3	125
CuO	Heated in an enclosed graphitic cylinder (1 torr) at 300 °C for 1 h	-0.75; 0; RHE; 1.5	138
C ₃ N ₄	Ground with LiCl/KCl mixture, followed by annealing at 550 °C for 24 h under N ₂ , then washing with HCl or NH ₃ solution	-0.5; 0; RHE; 5.0	139
Flame annealing			
CuFe ₂ O ₄	Annealed in an oxygen-rich flame region (>980 °C) for 16 min	-1.82; 0.4; RHE; 3.5	11
TiO ₂	Repeatedly spin-coated with precursor solution ten times and then heated in a <i>n</i> -butane flame for 25 s	1.17; 1.23; RHE; 4.5	127
Vacuum annealing			
ZnO	Annealed in vacuum (<1 mTorr) at 100–700 °C for 1 h	0.6; 1.23; RHE; 20	128
SnO ₂ /In ₂ O ₃	Annealed in an ultrahigh vacuum system (5 × 10 ⁻⁸ Pa)	N/A	21

^a Measured under infrared light (>800 nm). ^b Measured in 0.1 M phosphate buffer containing 0.1 M H₂O₂. ^c PVDF: polyvinylidene fluoride.

reduced charge transfer resistance, the as-prepared CuO exhibited a photocurrent density of -1.8 mA cm⁻² at 0.1 V vs. SHE, two times higher than that of the CuO annealed in synthetic air. Another work by Cen *et al.* examined the influence of annealing WO₃ under controlled oxygen pressure (95 mTorr).¹²¹ The treatment enhanced charge carrier density,

leading to a photocurrent density of 1.81 mA cm⁻² at 1.23 V vs. RHE, two times higher than that of untreated WO₃.

4.2 Other post-annealing treatments

4.2.1 Solid annealing.

In addition to gas-based post-annealing treatment, the reaction between photoelectrodes

and solid chemicals can be realized at a high temperature, known as solid-based annealing in the review. Gas annealing treatment seems to be a direct method to create unique surface structure to the materials; however, the choice of the gas is limited. Notably, the improper setup of gas annealing treatment is dangerous and fatal while using H_2 and NH_3 . Besides, various pressure applied in the annealing system offers different performance of the photoelectrode. In the following content, solid-based annealing, vacuum annealing, and flame annealing are introduced in addition to gas-based post-annealing treatment. These studies have been summarized in Table 5.

For example, Zhang *et al.* investigated the PEC properties of S-doped Fe_2O_3 nanorods.¹²⁴ Elemental S was doped in Fe_2O_3 by employing S powder upstream during the annealing process, similar to tube-furnace chemical vapor deposition. As a result of the enhanced electron mobility by the nonmetal doping, the S-doped Fe_2O_3 exhibited a photocurrent density of 1.42 mA cm^{-2} at 1.23 V vs. RHE . Rohloff *et al.* applied a low-cost solid-vapor reaction route to incorporate elemental F into $BiVO_4$ by annealing the photoanode close to F-rich organic polymers (PVDF) in an N_2 atmosphere (Fig. 11a).⁸ This F-modification treatment primarily affected the charge transfer efficiency at the $BiVO_4||\text{electrolyte}$ interface by increasing catalytic efficiency. In another study, by Xu *et al.*, metal-reduction methods—safer than hydrogenation—were used to reduce TiO_2 photoanodes.¹⁶ Among various metals such as Zn, Al, and Mg (Fig. 11b),

annealing with Mg powder could controllably alter the color of TiO_2 from light blue, to dark blue, and to black (Fig. 11c). The highest photocurrent density of the Mg-reduced TiO_2 photoanode attained 3.1 mA cm^{-2} at 1.0 V vs. RHE , five times higher than that of the bare one, owing to the generation of O_{vac} and Ti^{3+} species. Dong *et al.* explored co-doped strategies (Si/Ti^{3+} or Ni/Ti^{3+}) for improving the conductivity and charge transport of TiO_2 .^{125,126} In one study, after Zn metal reduction in argon at $700 \text{ }^\circ\text{C}$ for 4 h, the resultant black Si-doped TiO_2 exhibited a photocurrent density of 1.78 mA cm^{-2} at 0 V vs. Ag/AgCl , 5.1 and 1.9 times higher than that of bare TiO_2 and black Si-free TiO_2 , respectively.¹²⁵ Banerjee *et al.* reported the formation of an amorphous $Cu_{2-x}O$ overlayer for the passivation of CuO .¹³⁸ By annealing CuO in an enclosed graphitic cylinder at $300 \text{ }^\circ\text{C}$ for 30–120 min, the as-prepared $Cu_{2-x}O/Cu_2O/CuO$ exhibited a photocurrent density of -0.75 mA cm^{-2} at 0 V vs. RHE , 1.5 times higher than that of bare CuO . The enhanced photoactivity and stability were ascribed to the formation of a type II heterojunction and the beneficial electron trapping by the amorphous $Cu_{2-x}O$ overlayer. In another study, Wang *et al.* annealed carbon nitride with the presence of salts, including $CuCl_2$, KCl , and $LiCl$.¹³⁹ This salt-melt method not only introduced free $CuCl$ species that could act as type II heterostructure but only incorporated coordinated Cu atoms, which enhanced visible light absorption, resulting in a significantly improved PEC performance.

4.2.2 Flame annealing. As a special post-annealing strategy, flame treatments are endowed with the advantages of high temperature (easily to reach $1000 \text{ }^\circ\text{C}$), fast heating rate, and short process time. These studies have been summarized in Table 5.

Park *et al.* compared the effects of flame annealing with furnace annealing on a photocathode $CuFe_2O_4$ (Fig. 12a and b).⁴¹ The flame-treated $CuFe_2O_4$ exhibited a photocurrent density of 1.82 mA cm^{-2} at 0.4 V vs. RHE , 3.5 times higher than that of furnace-annealed $CuFe_2O_4$. The enhanced photoactivity was attributed to reduced bandgap which allowed more light absorption, increased porosity which enlarged the electrochemically active surface area (Fig. 12c and d) by a factor of 2.78, and eliminated O_{vac} which lowered undesirable charge recombination. Chen *et al.* explored the *ex situ* doping of TiO_2 by spin-coating W and Sn dopants on the photoanode followed by flame annealing.¹²⁷ The incorporation depth of Sn and W ions could be tuned by flame treatment time. Owing to the easy activation of water molecules by the co-existed W and Sn atoms, the flame-treated TiO_2 exhibited a 4.5-fold improvement in photoactivity, along with a cathodic shift of onset potential (450 mV).

4.2.3 Vacuum annealing. In addition to gas annealing, vacuum annealing sometimes results in unique changes of photoelectrodes. These studies have been summarized in Table 5.

For example, unfavorable hydroxyl groups at the surface of ZnO could be eliminated by post-annealing the photoanodes in a vacuum below 1 mTorr at $200\text{--}700 \text{ }^\circ\text{C}$.¹²⁸ Increasing the post-annealing temperature to $700 \text{ }^\circ\text{C}$ could induce the generation of O_{vac} , which acted as shallow donors and increased free charge carrier density. Consequently, the as-annealed ZnO exhibited

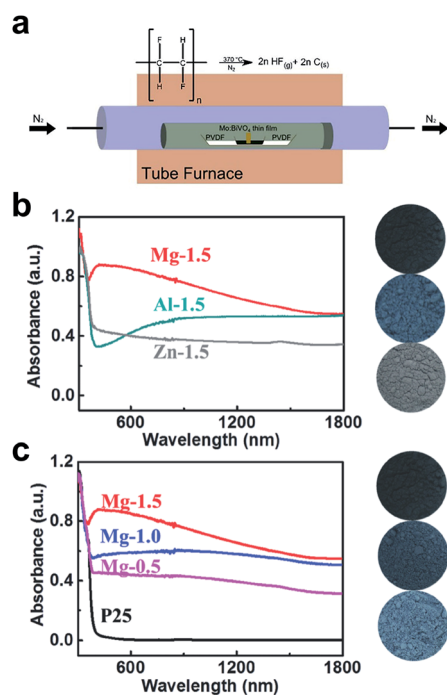


Fig. 11 (a) Schematic illustration of the synthesis of F-incorporated $BiVO_4$.⁸ Reprinted with permission from ref. 8, copyright 2019 American Chemical Society. (b and c) UV-visible absorption spectra and corresponding digital photographs of colored TiO_2 reduced by (b) various metals and (c) various dosages of Mg.¹⁶ Reprinted with permission from ref. 16, copyright 2017 The Royal Society of Chemistry.

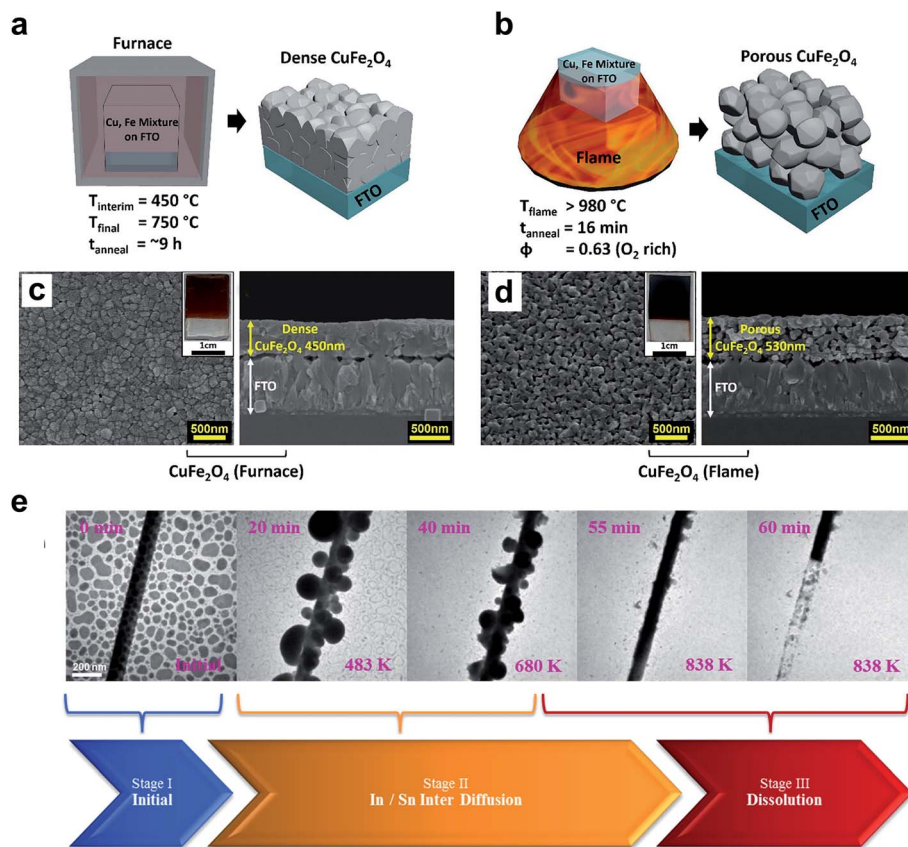


Fig. 12 (a and b) Schematic illustration of CuFe_2O_4 on FTO annealed by (a) furnace annealing conditions with the formation of dense film and (b) flame annealing conditions with the formation of the porous structure. (c and d) Top and cross-section SEM images of the (c) furnace-annealed CuFe_2O_4 and (d) flame-annealed CuFe_2O_4 .¹¹ Modified with permission from ref. 11, copyright 2019 American Chemical Society. (e) A series of *in situ* TEM images of indium metal/ SnO_2 nanowires during annealing in an ultra-high vacuum system.²¹ Reprinted with permission from ref. 21, copyright 2018 Elsevier Ltd.

a photocurrent density of 0.6 mA cm^{-2} at 1.23 V vs. RHE , 20 times higher than that of untreated ZnO. In another report by Liu *et al.*,²¹ the $\text{SnO}_2/\text{In}_2\text{O}_3$ heterojunction was heated in the vacuum range from 100 Pa in the air to $5 \times 10^{-8} \text{ Pa}$, which determined the amount of O_{vac} . *In situ* TEM observation was performed to explore detailed changes during annealing (Fig. 12e). The creation of O_{vac} in the vacuum-annealed $\text{SnO}_{2-x}/\text{In}_2\text{O}_{3-y}$ photoelectrode should be responsible for the 1.6-fold increase in H_2 production.

5. Summary and outlook

The preparation of efficient and robust semiconductor photoelectrodes by facile post-synthetic treatments could accelerate the potentially industrial PEC water splitting application for the development of sustainable energy conversion technology. This review summarizes advances in post-synthetic treatments for PEC applications reported in this field in the past five years, focusing on the details of the various post-treatment methods and the resultant improved PEC performance. Various effective strategies, of which most are surface modification methods, have also been introduced. Despite that the great progress has been made in developing post-synthetic treatment methods for

improving photoelectrodes, there is still considerable distance to go before the industrial-scale application of PEC water splitting. The following is a detailed discussion of current limitations, challenges and prospects for future development in the field of post-treatments of photoelectrodes for PEC water splitting technology.

First, it is worthy to notice that the PEC stability of the resultant post-treated photoelectrodes is, from time to time, not satisfactory. The photoactivity of chemically treated photoelectrodes, such as borate-treated BiVO_4 ,¹⁹ can be reversed or easily undermined alongside the PEC measurement process in just a few hours. Another typical example is that illuminating BiVO_4 photoanodes under open-circuit conditions can enhance PEC photoactivity, but the photoanode standing still in the electrolyte overnight can undesirably lead to the receding of photocurrent density to its initial level.⁵ Thus, it is of significance for researchers to explore the intrinsic properties of post-treatment-induced surface structure changes and think of useful methods by which to avoid the diminishing of these functional structures, such as by coating protective/passivation/cocatalyst layers, in the pursuit of long-term stability.

Although chemical treatment is a facile, efficient and low-cost method to change the defect chemistry at the surface and

in the bulk of semiconductor, it has an obvious limitation on material choice. The main target for chemical reduction method is to create oxygen vacancies on the surface of the metal oxide. Metal ions that are easily to be reduced may not be applicable. The misuse of chemical reduction method can damage the crystallinity of the materials. As reported, electrochemical treatments on the photoelectrode can be quantitatively controlled, so that researchers could modify the material in a more precise scale. However, the operational parameters, such as an applied potential and the corresponding electrolyte, were complex and totally different unless same material has been used. Such unclear and limited record on electrochemical treatments can restrict the progress by using electrochemical treatments. An in-depth investigation, *e.g.*, *in situ* X-ray diffraction pattern analysis and *in situ* Raman spectrometer analysis, of photoelectrodes using electrochemical treatments can help scientists to understand the kinetics and dynamics of electrochemical treatments. Irradiation-based treatment has an obvious limitation on its slow treatment process. In the normal cases, it requires 10 hour irradiation. Some methodologies require the treatment process work under open-circuit condition. A 248 nm pulse laser can effectively reduce the irradiation duration from hours to seconds, but it is a high-cost solution. Post-annealing treatment is a very high-cost method. During the process, it consumes a lot of gas. Some preparation method is dangerous, for instance, hydrogen annealing treatment. The leak of gas into the H₂-filled furnace tube can cause explosion. Solid-based annealing may cause contamination to the tube due to evaporation of solid sample. Frequent replacement of quartz tubes can greatly increase the cost.

Post-synthetically modified surface structure changes in photoelectrodes can directly interact with electrolytes, in a manner similar to the electrolysis of water. As an important component in a PEC system, electrolytes and their impact on PEC performance undeniably cannot be ignored. It has been reported that the composition and chemical properties (*e.g.*, pH) of electrolytes have tremendous impacts.^{9,22,140–145} For example, the relation between PEC performance and the variation of electrolyte composition has been investigated for BiVO₄ photoanodes, proving that the pH and cation size significantly influence the solar water oxidation reaction.¹⁴¹ In addition, during the PEC process, various intermediates may be generated when employing different electrolytes, and the one that primarily influences OER/HER efficiencies should be explored.

It is usually envisioned that post-synthetic treatments for surface modification should only alter the surface properties of metal oxide photoanodes. However, from time to time, the bulk properties, such as light absorption and charge separation efficiencies, could be improved or impaired. It is of interest and significance to explore the reasons why surface structural changes or surface state alternations have such great influence on these bulk structures, in order to gain an in-depth understanding of the structure–property–performance relationships.

A large number of post-treatments exclusively influence the surface physicochemical properties of photoelectrodes. Thus, it is important to develop cutting-edge techniques by which to precisely characterize surface chemistry changes; for example,

the destruction of chemical bonds and the formation of new bonds is of critical importance for a deep understanding of the roles of surface atomic arrangements. Furthermore, it is worth noting that the illumination involved during PEC measurements makes it harder to capture such changes, as some alternations might be easily reverted back to initial states. Thus, *in situ* techniques that provide opportunities to observe these possibly generated structure changes should be promoted. The development of such techniques can also broaden our understanding of the relation between photocorrosion and irradiation treatments, a field that is inadequately studied at the moment, because of a lack of understanding of the detailed impact of irradiation on photoelectrode surfaces and bulk structures. Without such knowledge, applying these post-treatments to improve the performance and stability of photoelectrodes in a pertinent manner seems to be difficult. Accordingly, in addition to photo-responsive semiconductor materials, an in-depth understanding of the photophysical (*e.g.*, light absorption, and charge formation, and charge separation) and photoelectrochemical (*e.g.*, photoredox activity, electrochemical resistance, and diffusion behaviors) properties of solid/solid and solid/liquid interfaces are suggested to be achieved by utilizing *in situ* characterization techniques under dark and light conditions, which will definitely provide new insights into the advancement of next-generation PEC semiconductor materials for commercial applications in the emerging field of electrocatalytic, photocatalytic, and photoelectrocatalytic technologies.

Conflicts of interest

There are no conflicts to declare.

Acknowledgements

The authors acknowledge financial support from the Research Grants Council of Hong Kong (grant no. 21203518, F-CityU106/18 and 9048121), City University of Hong Kong (grant no. 9667229, 7005289, 7005580, 7005720, 9680208, 9667213 and 9052029), and Shenzhen Science Technology and Innovation Commission (grant no. R-IND12302 and R-IND12303), as well as National Natural Science Foundation of China (grant no. 51701159). X. Zou would like to thank the National Natural Science Foundation of China (grant no. 52022054 and 51974181), the Shanghai Rising-Star Program (19QA1403600), and the Program for Professor of Special Appointment (Eastern Scholar) at Shanghai Institutions of Higher Learning (TP2019041) for financial support.

References

- 1 J. Xiao, F. Zhao, J. Zhong, Z. Huang, L. Fan, L. Peng, S.-F. Zhou and G. Zhan, *Chem. Eng. J.*, 2020, **402**, 126163.
- 2 L. Shi, W. Zhou, Z. Li, S. Koul, A. Kushima and Y. Yang, *ACS Nano*, 2018, **12**, 6335–6342.

- 3 K. Zhang, S. Ravishankar, M. Ma, G. Veerappan, J. Bisquert, F. Fabregat-Santiago and J. H. Park, *Adv. Energy Mater.*, 2017, **7**, 1600923.
- 4 S. Wang, P. Chen, J. H. Yun, Y. Hu and L. Wang, *Angew. Chem., Int. Ed.*, 2017, **56**, 8500–8504.
- 5 B. J. Trzeźniewski and W. A. Smith, *J. Mater. Chem. A*, 2016, **4**, 2919–2926.
- 6 J. Xie, P. Yang, X. Liang and J. Xiong, *ACS Appl. Energy Mater.*, 2018, **1**, 2769–2775.
- 7 J. Zhang, X. Chang, C. Li, A. Li, S. Liu, T. Wang and J. Gong, *J. Mater. Chem. A*, 2018, **6**, 3350–3354.
- 8 M. Rohloff, B. r. Anke, O. Kasian, S. Zhang, M. Lerch, C. Scheu and A. Fischer, *ACS Appl. Mater. Interfaces*, 2019, **11**, 16430–16442.
- 9 B. J. Trzeźniewski, I. A. Digdaya, T. Nagaki, S. Ravishankar, I. Herraiz-Cardona, D. A. Vermaas, A. Longo, S. Gimenez and W. A. Smith, *Energy Environ. Sci.*, 2017, **10**, 1517–1529.
- 10 M. Wang, X. Wu, K. Huang, Y. Sun, Y. Zhang, H. Zhang, J. He, H. Chen, J. Ding and S. Feng, *Nanoscale*, 2018, **10**, 6678–6683.
- 11 S. Park, J. H. Baek, L. Zhang, J. M. Lee, K. H. Stone, I. S. Cho, J. Guo, H. S. Jung and X. Zheng, *ACS Sustainable Chem. Eng.*, 2019, **7**, 5867–5874.
- 12 J. Xiao, L. Fan, F. Zhao, Z. Huang, S.-F. Zhou and G. Zhan, *J. Catal.*, 2020, **381**, 139–149.
- 13 P. Varadhan, H.-C. Fu, D. Priante, J. R. D. Retamal, C. Zhao, M. Ebaid, T. K. Ng, I. Ajia, S. Mitra, I. S. Roqan, B. S. Ooi and J.-H. He, *Nano Lett.*, 2017, **17**, 1520–1528.
- 14 J. K. Kim, Y. Cho, M. J. Jeong, B. Levy-Wendt, D. Shin, Y. Yi, D. H. Wang, X. Zheng and J. H. Park, *ChemSusChem*, 2018, **11**, 933–940.
- 15 D. Cibrev, M. Tallarida, C. Das, T. Lana-Villarreal, D. Schmeisser and R. Gómez, *Phys. Chem. Chem. Phys.*, 2017, **19**, 21807–21817.
- 16 J. Xu, Z. Tian, G. Yin, T. Lin and F. Huang, *Dalton Trans.*, 2017, **46**, 1047–1051.
- 17 Y. He, P. Wang, J. Zhu, Y. Yang, Y. Liu, M. Chen, D. Cao and X. Yan, *ACS Appl. Mater. Interfaces*, 2019, **11**, 37322–37329.
- 18 S. Tamura, K. Ueno and K. Hato, *Mater. Res. Bull.*, 2019, **112**, 221–225.
- 19 Q. Meng, B. Zhang, L. Fan, H. Liu, M. Valvo, K. Edström, M. Cuartero, R. De Marco, G. A. Crespo and L. Sun, *Angew. Chem., Int. Ed.*, 2019, **58**, 19027–19033.
- 20 J. Deng, X. Lv and J. Zhong, *J. Phys. Chem. C*, 2018, **122**, 29268–29273.
- 21 W.-T. Liu, B.-H. Wu, Y.-T. Lai, N.-H. Tai, T.-P. Perng and L.-J. Chen, *Nano Energy*, 2018, **47**, 18–25.
- 22 N. J. Firet, A. Venugopal, M. A. Blommaert, C. Cavallari, C. J. Sahle, A. Longo and W. A. Smith, *Chem. Mater.*, 2019, **31**, 7453–7462.
- 23 X. Feng, R. Li, M. Wang and Y. Chen, *J. Mater. Chem. A*, 2018, **6**, 11180–11188.
- 24 Z. Wang, L. Zhang, T. U. Schüllli, Y. Bai, S. A. Monny, A. Du and L. Wang, *Angew. Chem., Int. Ed.*, 2019, **58**, 17604–17609.
- 25 A. Y. Ru Ng, B. Boruah, K. F. Chin, J. M. Modak and H. S. Soo, *ChemNanoMat*, 2020, **6**, 185–203.
- 26 F. Dawood, M. Anda and G. Shafiullah, *Int. J. Hydrogen Energy*, 2020, **45**, 3847–3869.
- 27 K. Maeda and K. Domen, *J. Phys. Chem. Lett.*, 2010, **1**, 2655–2661.
- 28 A. Fujishima and K. Honda, *Nature*, 1972, **238**, 37–38.
- 29 Y. Yang, S. Niu, D. Han, T. Liu, G. Wang and Y. Li, *Adv. Energy Mater.*, 2017, **7**, 1700555.
- 30 J. Zhao, H. Yin, T. Lim, H. Xie, H.-Y. Hsu, F. Forouzan and A. J. Bard, *J. Electrochem. Soc.*, 2016, **163**, D506–D514.
- 31 J. H. Kim and J. S. Lee, *Adv. Mater.*, 2019, **31**, 1806938.
- 32 Y. Chen, X. Feng, Y. Liu, X. Guan, C. Burda and L. Guo, *ACS Energy Lett.*, 2020, **5**, 844–866.
- 33 T. Lopes, P. Dias, L. Andrade and A. Mendes, *Sol. Energy Mater. Sol. Cells*, 2014, **128**, 399–410.
- 34 B. Yao, J. Zhang, X. Fan, J. He and Y. Li, *Small*, 2019, **15**, 1803746.
- 35 H.-Y. Liu, C. C. Cody, J. A. Jacob-Dolan, R. H. Crabtree and G. W. Brudvig, *ACS Energy Lett.*, 2020, **5**, 3195–3202.
- 36 Z. Zhang and J. T. Yates Jr, *Chem. Rev.*, 2012, **112**, 5520–5551.
- 37 L. Zheng, X. Ye, X. Deng, Y. Wang, Y. Zhao, X. Shi and H. Zheng, *ACS Sustainable Chem. Eng.*, 2020, **8**, 15906–15914.
- 38 L. Shi, Z. Li, T. D. Dao, T. Nagao and Y. Yang, *J. Mater. Chem. A*, 2018, **6**, 12978–12984.
- 39 J. Li, L. Guo, N. Lei, Q. Song and Z. Liang, *ChemElectroChem*, 2017, **4**, 2852–2861.
- 40 A. Liao, H. He, Z. Fan, G. Xu, L. Li, J. Chen, Q. Han, X. Chen, Y. Zhou and Z. Zou, *J. Catal.*, 2017, **352**, 113–119.
- 41 R. Liu, X. Peng, X. Han, C. H. Mak, K.-C. Cheng, S. P. Santoso, H.-H. Shen, Q. Ruan, F. Cao and T. Y. Edward, *J. Electroanal. Chem.*, 2021, **887**, 115167.
- 42 J. Li, Z. Liang, L. Guo, N. Lei and Q. Song, *Mater. Lett.*, 2018, **223**, 93–96.
- 43 M. Kim, B. Lee, H. Ju, J. Y. Kim, J. Kim and S. W. Lee, *Adv. Mater.*, 2019, **31**, 1903316.
- 44 J. U. Kim, H. S. Han, J. Park, W. Park, J. H. Baek, J. M. Lee, H. S. Jung and I. S. Cho, *J. Catal.*, 2018, **365**, 138–144.
- 45 Y. Liu, Y. Yang, Q. Liu, H. He, W. Liu, D. Meng, Y. Li, W. Li and J. Li, *Int. J. Hydrogen Energy*, 2018, **43**, 208–218.
- 46 Q. Yang, J. Du, J. Li, Y. Wu, Y. Zhou, Y. Yang, D. Yang and H. He, *ACS Appl. Mater. Interfaces*, 2020, **12**, 11625–11634.
- 47 Y. Peng, H. Wu, M. Yuan, F.-F. Li, X. Zou, Y. H. Ng and H.-Y. Hsu, *Sustainable Energy Fuels*, 2021, **5**, 2284–2293.
- 48 X. Long, F. Li, L. Gao, Y. Hu, H. Hu, J. Jin and J. Ma, *ChemSusChem*, 2018, **11**, 4094–4101.
- 49 Y. Yang, M. Forster, Y. Ling, G. Wang, T. Zhai, Y. Tong, A. J. Cowan and Y. Li, *Angew. Chem., Int. Ed.*, 2016, **55**, 3403–3407.
- 50 Q. Wu, D. Meng, Y. Zhang, Q. Zhao, Q. Bu, D. Wang, X. Zou, Y. Lin, S. Li and T. Xie, *J. Alloys Compd.*, 2019, **782**, 943–951.
- 51 D. Cao, W. Luo, J. Feng, X. Zhao, Z. Li and Z. Zou, *Energy Environ. Sci.*, 2014, **7**, 752–759.
- 52 X. Zhang, X. Wang, X. Yi, J. Ye and D. Wang, *ACS Sustainable Chem. Eng.*, 2019, **7**, 5420–5429.
- 53 D. Zheng, X. He, W. Xu and X. Lu, *Mater. Res. Bull.*, 2017, **96**, 354–359.

- 54 Y. Mao, C. Ning, N. Zhang, Y. Hu, M. Li, H. Yang, S. Chen, S. Su and E. Liang, *J. Electrochem. Soc.*, 2018, **165**, H799–H803.
- 55 Z. Ma, A. Jaworski, J. George, A. Rokicinska, T. Thersleff, T. M. Budnyak, G. Hautier, A. J. Pell, R. Dronskowski, P. Kuśtrowski and A. Slabon, *J. Phys. Chem. C*, 2019, **124**, 152–160.
- 56 M. A. Rahman, J. P. Thomas and K. T. Leung, *Adv. Energy Mater.*, 2018, **8**, 1701234.
- 57 J. Deng, X. Lv, K. Nie, X. Lv, X. Sun and J. Zhong, *ACS Catal.*, 2017, **7**, 4062–4069.
- 58 G. Liu, Y. Zhao, N. Li, R. Yao, M. Wang, Y. Wu, F. Zhao and J. Li, *Electrochim. Acta*, 2019, **307**, 197–205.
- 59 T. K. Sahu, A. K. Shah, A. Banik and M. Qureshi, *ACS Appl. Energy Mater.*, 2019, **2**, 4325–4334.
- 60 M. Favaro, F. F. Abdi, M. Lamers, E. J. Crumlin, Z. Liu, R. van de Krol and D. E. Starr, *J. Phys. Chem. B*, 2018, **122**, 801–809.
- 61 Y. Liu, B. R. Wygant, O. Mabayoje, J. Lin, K. Kawashima, J.-H. Kim, W. Li, J. Li and C. B. Mullins, *ACS Appl. Mater. Interfaces*, 2018, **10**, 12639–12650.
- 62 J. Xu, Z. Hu, J. Zhang, W. Xiong, L. Sun, L. Wan, R. Zhou, Y. Jiang and C.-S. Lee, *J. Mater. Chem. A*, 2017, **5**, 25230–25236.
- 63 R. Chong, Y. Du, Z. Chang, Y. Jia, S. Liu, Y. Liu, Y. Zhou and D. Li, *Appl. Catal., B*, 2019, **250**, 224–233.
- 64 H.-Q. Chen, L.-Y. Lin and S.-L. Chen, *ACS Appl. Energy Mater.*, 2018, **1**, 6089–6100.
- 65 A. Brayek, S. Chaguetmi, M. Ghoul, I. B. Assaker, R. Chtourou, P. Decorse, P. Beaunier, S. Nowak, F. Mammeri and S. Ammar, *RSC Adv.*, 2018, **8**, 11785–11798.
- 66 Y. Li, J. Liu, X. Li, X. Wan, R. Pan, H. Rong, J. Liu, W. Chen and J. Zhang, *ACS Appl. Mater. Interfaces*, 2019, **11**, 27170–27177.
- 67 N. Liu, C. Schneider, D. Freitag, M. Hartmann, U. Venkatesan, J. Müller, E. Spiecker and P. Schmuki, *Nano Lett.*, 2014, **14**, 3309–3313.
- 68 M. Chiesa, M. C. Paganini, S. Livraghi and E. Giamello, *Phys. Chem. Chem. Phys.*, 2013, **15**, 9435–9447.
- 69 C. Zhang, R. Liu, C. H. Mak, X. Zou, H.-H. Shen, S.-Y. Leu, L. Ji and H.-Y. Hsu, *J. Photonics Energy*, 2018, **8**, 021001.
- 70 S. Hoang, S. Guo, N. T. Hahn, A. J. Bard and C. B. Mullins, *Nano Lett.*, 2012, **12**, 26–32.
- 71 Y. Yan, M. Han, A. Konkin, T. Koppe, D. Wang, T. Andreu, G. Chen, U. Vetter, J. R. Morante and P. Schaaf, *J. Mater. Chem. A*, 2014, **2**, 12708–12716.
- 72 Z. Chen, H.-Y. Hsu, M. Arca and K. S. Schanze, *J. Phys. Chem. B*, 2014, **119**, 7198–7209.
- 73 Y. Peng, Q. Ruan, C. H. Lam, F. Meng, C.-Y. Guan, S. P. Santoso, X. Zou, T. Y. Edward, P. K. Chu and H.-Y. Hsu, *J. Alloys Compd.*, 2021, **870**, 159376.
- 74 N. Liu, V. Häublein, X. Zhou, U. Venkatesan, M. Hartmann, M. Mačković, T. Nakajima, E. Spiecker, A. Osvet, L. Frey and P. Schmuki, *Nano Lett.*, 2015, **15**, 6815–6820.
- 75 H. Cui, W. Zhao, C. Yang, H. Yin, T. Lin, Y. Shan, Y. Xie, H. Gu and F. Huang, *J. Mater. Chem. A*, 2014, **2**, 8612–8616.
- 76 J. Song, M. Zheng, X. Yuan, Q. Li, F. Wang, L. Ma, Y. You, S. Liu, P. Liu, D. Jiang, L. Ma and W. Shen, *J. Mater. Sci.*, 2017, **52**, 6976–6986.
- 77 H. Zhu, M. Zhao, J. Zhou, W. Li, H. Wang, Z. Xu, L. Lu, L. Pei, Z. Shi, S. Yan, Z. Li and Z. Zou, *Appl. Catal., B*, 2018, **234**, 100–108.
- 78 Y. Fang, Y. Ma and X. Wang, *Chin. J. Catal.*, 2018, **39**, 438–445.
- 79 T. Li and D. Ding, *J. Electroanal. Chem.*, 2020, **167**, 066514.
- 80 I. Constantinou, T. H. Lai, H. Y. Hsu, S. H. Cheung, E. D. Klump, K. S. Schanze, S. K. So and F. So, *Adv. Electron. Mater.*, 2015, **1**, 1500167.
- 81 J. Liu, M. Dai, J. Wu, Y. Hu, Q. Zhang, J. Cui, Y. Wang, H. H. Tan and Y. Wu, *Sci. Bull.*, 2018, **63**, 194–202.
- 82 G. Wang, Y. Yang, Y. Ling, H. Wang, X. Lu, Y.-C. Pu, J. Z. Zhang, Y. Tong and Y. Li, *J. Mater. Chem. A*, 2016, **4**, 2849–2855.
- 83 Y. Bu, J. Tian, Z. Chen, Q. Zhang, W. Li, F. Tian and J. P. Ao, *Adv. Mater. Interfaces*, 2017, **4**, 1601235.
- 84 H. Zhang, J. H. Park, W. J. Byun, M. H. Song and J. S. Lee, *Chem. Sci.*, 2019, **10**, 10436–10444.
- 85 S. Zhang, Z. Zhang and W. Leng, *Phys. Chem. Chem. Phys.*, 2020, **22**, 7835–7843.
- 86 D. Cao, H. Xiao, Q. Gao, X. Yang, C. Luan, H. Mao, J. Liu and X. Liu, *Nanoscale*, 2017, **9**, 11504–11510.
- 87 A. Goryachev, L. Gao, R. P. J. van Veldhoven, J. E. M. Haverkort, J. P. Hofmann and E. J. M. Hensen, *Phys. Chem. Chem. Phys.*, 2018, **20**, 14242–14250.
- 88 H.-Y. Hsu, L. Ji, M. Du, J. Zhao, T. Y. Edward and A. J. Bard, *Electrochim. Acta*, 2016, **220**, 205–210.
- 89 T. Li, J. He, B. Peña and C. P. Berlinguette, *Angew. Chem., Int. Ed.*, 2016, **55**, 1769–1772.
- 90 E. Y. Liu, J. E. Thorne, Y. He and D. Wang, *ACS Appl. Mater. Interfaces*, 2017, **9**, 22083–22087.
- 91 S. Feng, T. Wang, B. Liu, C. Hu, L. Li, Z. J. Zhao and J. Gong, *Angew. Chem., Int. Ed.*, 2020, **59**, 2044–2048.
- 92 X. Zou, L. Ji, H.-Y. Hsu, K. Zheng, Z. Pang and X. Lu, *J. Mater. Chem. A*, 2018, **6**, 12724–12732.
- 93 X. Yin, J. Li, L. Du, F. Zhan, K. Kawashima, W. Li, W. Qiu, Y. Liu, X. Yang, K. Wang, Y. Ning and C. B. Mullins, *ACS Appl. Energy Mater.*, 2020, **3**, 4403–4410.
- 94 T. Li, J. He, B. Peña and C. P. Berlinguette, *ACS Appl. Mater. Interfaces*, 2016, **8**, 25010–25013.
- 95 A. G. Breuhaus-Alvarez, J. L. DiMeglio, J. J. Cooper, C. R. Lhermitte and B. M. Bartlett, *J. Phys. Chem. C*, 2019, **123**, 1142–1150.
- 96 A. Venugopal and W. A. Smith, *Faraday Discuss.*, 2019, **215**, 175–191.
- 97 Y. Xu, M. A. Melia, L.-k. Tsui, J. M. Fitz-Gerald and G. Zangari, *J. Phys. Chem. C*, 2017, **121**, 17121–17128.
- 98 S. K. Cushing, F. Meng, J. Zhang, B. Ding, C. K. Chen, C.-J. Chen, R.-S. Liu, A. D. Bristow, J. Bright, P. Zheng and N. Wu, *ACS Catal.*, 2017, **7**, 1742–1748.
- 99 S. Yan, T. Liu, Y. Zhang, D. Sun, X. Li, G. Xie, C. Feng and L. Xu, *J. Electroanal. Chem.*, 2017, **807**, 213–219.

- 100 J. H. Kim, Y. J. Jang, S. H. Choi, B. J. Lee, J. H. Kim, Y. B. Park, C.-M. Nam, H. G. Kim and J. S. Lee, *J. Mater. Chem. A*, 2018, **6**, 12693–12700.
- 101 Z. Gu, L. Zhang, B. Wen, X. An, H. Lan, L.-M. Liu, T. Chen, J. Zhang, X. Cao, J. Tang, H. Liu and J. Qu, *Nano Energy*, 2018, **53**, 887–897.
- 102 Y. Ma, B. Feng, J. Lang, F. Wang and Y. H. Hu, *J. Phys. Chem. C*, 2019, **123**, 25833–25843.
- 103 C. Dong, Y. Wang, H. Wang, C. S. K. Lin, H.-Y. Hsu and S.-Y. Leu, *Energy Procedia*, 2019, **158**, 918–925.
- 104 T.-H. Lai, I. Constantinou, C. M. Grand, E. D. Klump, S. Baek, H.-Y. Hsu, S.-W. Tsang, K. S. Schanze, J. R. Reynolds and F. So, *Chem. Mater.*, 2016, **28**, 2433–2440.
- 105 S. Mohajernia, S. Hejazi, A. Mazare, N. T. Nguyen and P. Schmuki, *Chem.–Eur. J.*, 2017, **23**, 12406–12411.
- 106 Y. Xu, Q. Lin, R. Ahmed, E. R. Hoglund and G. Zangari, *J. Power Sources*, 2019, **410**, 59–68.
- 107 N. Liu, C. Schneider, D. Freitag, E. M. Zolnhofer, K. Meyer and P. Schmuki, *Chem.–Eur. J.*, 2016, **22**, 13810–13814.
- 108 M. Kodera, Y. Moriya, M. Katayama, T. Hisatomi, T. Minegishi and K. Domen, *Sci. Rep.*, 2018, **8**, 1–10.
- 109 H. Zhang, L. Ma, J. Ming, B. Liu, Y. Zhao, Y. Hou, Z. Ding, C. Xu, Z. Zhang and J. Long, *Appl. Catal., B*, 2019, **243**, 481–489.
- 110 C. H. Mak, X. Huang, R. Liu, Y. Tang, X. Han, L. Ji, X. Zou, G. Zou and H.-Y. Hsu, *Nano Energy*, 2020, 104752.
- 111 H.-Y. Hsu, H.-H. Hsieh, H.-Y. Tuan and J.-L. Hwang, *Sol. Energy Mater. Sol. Cells*, 2010, **94**, 955–959.
- 112 S. Rao, X. Zou, S. Wang, T. Shi, Y. Lu, L. Ji, H.-Y. Hsu, Q. Xu and X. Lu, *J. Electrochem. Soc.*, 2019, **166**, D427.
- 113 P. K. Das, M. Arunachalam, K. R. Subhash, Y. J. Seo, K.-S. Ahn, J.-S. Ha and S. H. Kang, *Dalton Trans.*, 2020, **49**, 15023–15033.
- 114 Y. Xu, R. Ahmed, D. Klein, S. Cap, K. Freedy, S. McDonnell and G. Zangari, *J. Power Sources*, 2019, **414**, 242–249.
- 115 X. Lv, L. Tao, M. Cao, X. Xiao, M. Wang and Y. Shen, *Nano Energy*, 2018, **44**, 411–418.
- 116 C. H. Mak, X. Han, M. Du, J.-J. Kai, K. F. Tsang, G. Jia, K.-C. Cheng, H.-H. Shen and H.-Y. Hsu, *J. Mater. Chem. A*, 2021, **9**, 4454–4504.
- 117 R. Irani, I. Y. Ahmet, J.-W. Jang, S. P. Berglund, P. Plate, C. Höhn, R. Böttger, S. W. Schmitt, C. Dubourdieu, S. Lardhi, L. Cavallo, M. Harb, P. Bogdanoff, R. van de Krol and F. F. Abdi, *Sol. RRL*, 2020, **4**, 1900290.
- 118 J. Seo, M. Nakabayashi, T. Hisatomi, N. Shibata, T. Minegishi, M. Katayama and K. Domen, *J. Mater. Chem. A*, 2019, **7**, 493–502.
- 119 J. Seo, T. Hisatomi, M. Nakabayashi, N. Shibata, T. Minegishi, M. Katayama and K. Domen, *Adv. Energy Mater.*, 2018, **8**, 1800094.
- 120 W. Zhang, L. Song, J. Cen and M. Liu, *J. Phys. Chem. C*, 2019, **123**, 20730–20736.
- 121 J. Cen, Q. Wu, D. Yan, W. Zhang, Y. Zhao, X. Tong, M. Liu and A. Orlov, *RSC Adv.*, 2019, **9**, 899–905.
- 122 H.-Y. Hsu, L. Ji, C. Zhang, C. H. Mak, R. Liu, T. Wang, X. Zou, S.-Y. Leu and E. T. Yu, *J. Mater. Chem. C*, 2018, **6**, 11552–11560.
- 123 H. Lim, J. L. Young, J. F. Geisz, D. J. Friedman, T. G. Deutsch and J. Yoon, *Nat. Commun.*, 2019, **10**, 1–9.
- 124 R. Zhang, Y. Fang, T. Chen, F. Qu, Z. Liu, G. Du, A. M. Asiri, T. Gao and X. Sun, *ACS Sustainable Chem. Eng.*, 2017, **5**, 7502–7506.
- 125 Z. Dong, D. Ding, T. Li and C. Ning, *RSC Adv.*, 2018, **8**, 5652–5660.
- 126 Z. Dong, D. Ding, T. Li and C. Ning, *Appl. Surf. Sci.*, 2019, **480**, 219–228.
- 127 B. Chen, B. Ge, S. Fu, Q. Li, X. Chen, L. Li, J. Wang, Z. Yang, J. Ding, W. Fan, B. Mao and W. Shi, *Chem. Eng. Sci.*, 2020, **226**, 115843.
- 128 M. Baek, D. Kim and K. Yong, *ACS Appl. Mater. Interfaces*, 2017, **9**, 2317–2325.
- 129 Z. Luo, C. Li, S. Liu, T. Wang and J. Gong, *Chem. Sci.*, 2017, **8**, 91–100.
- 130 X. Chen, L. Liu, Y. Y. Peter and S. S. Mao, *Science*, 2011, **331**, 746–750.
- 131 G. Wang, H. Wang, Y. Ling, Y. Tang, X. Yang, R. C. Fitzmorris, C. Wang, J. Z. Zhang and Y. Li, *Nano Lett.*, 2011, **11**, 3026–3033.
- 132 Z. Zheng, B. Huang, J. Lu, Z. Wang, X. Qin, X. Zhang, Y. Dai and M.-H. Whangbo, *Chem. Commun.*, 2012, **48**, 5733–5735.
- 133 C. H. Mak, R. Liu, X. Han, Y. Tang, X. Zou, H. H. Shen, Y. Meng, G. Zou and H. Y. Hsu, *Adv. Opt. Mater.*, 2020, **8**, 2001023.
- 134 R. Liu, C. H. Mak, X. Han, Y. Tang, G. Jia, K.-C. Cheng, H. Qi, X. Zou, G. Zou and H.-Y. Hsu, *J. Mater. Chem. A*, 2020, **8**, 23803–23811.
- 135 Y. Tang, C. H. Mak, R. Liu, Z. Wang, L. Ji, H. Song, C. Tan, F. Barrière and H. Y. Hsu, *Adv. Funct. Mater.*, 2020, 2006919.
- 136 N. Liu, C. Schneider, D. Freitag, U. Venkatesan, V. R. R. Marthala, M. Hartmann, B. Winter, E. Spiecker, A. Osvet, E. M. Zolnhofer, K. Meyer, T. Nakajima, X. Zhou and P. Schmuki, *Angew. Chem., Int. Ed.*, 2014, **53**, 14201–14205.
- 137 D. Liu, C. Wang, Y. Yu, B.-H. Zhao, W. Wang, Y. Du and B. Zhang, *Chem*, 2019, **5**, 376–389.
- 138 S. Banerjee, F. Wu, Y. Myung, S. Chatman, D. M. Niedzwiedzki and P. Banerjee, *J. Electrochem. Soc.*, 2018, **165**, H417–H424.
- 139 Z. Wang, B. Jin, G. Zou, K. Zhang, X. Hu and J. H. Park, *ChemSusChem*, 2019, **12**, 866–872.
- 140 C.-F. Liu, Y.-J. Lu and C.-C. Hu, *ACS Omega*, 2018, **3**, 3429–3439.
- 141 P. K. Das, M. Arunachalam, Y. J. Seo, K.-S. Ahn, J.-S. Ha and S. H. Kang, *J. Electroanal. Chem.*, 2019, **842**, 41–49.
- 142 M. Tayebi, A. Tayyebi, T. Soltani and B.-K. Lee, *New J. Chem.*, 2019, **43**, 9106–9115.
- 143 S. Zhang, I. Ahmet, S.-H. Kim, O. Kasian, A. M. Mingers, P. Schnell, M. Kölbach, J. Lim, A. Fischer, K. J. J. Mayrhofer, S. Cherevko, B. Gault, R. van de Krol and C. Scheu, *ACS Appl. Energy Mater.*, 2020, **3**, 9523–9527.
- 144 K. Oh, V. Dorcet, B. Fabre and G. Loget, *Adv. Energy Mater.*, 2020, **10**, 1902963.
- 145 R. T. Gao and L. Wang, *Angew. Chem., Int. Ed.*, 2020, **59**, 23094–23099.